

STUDY OF RADIATION DAMAGE IN STAINLESS STEEL
BY COULOMB-EXCITED MOSSBAUER SPECTROSCOPY

by

JAMES NILS WICKBERG

B. S. in Physics, Oklahoma University, 1974

A MASTER'S THESIS

submitted in partial fulfillment of the
requirements for the degree

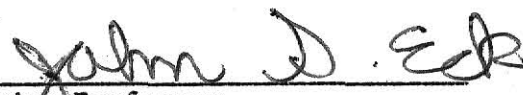
MASTER OF SCIENCE

Department of Physics

KANSAS STATE UNIVERSITY
Manhattan, Kansas

1977

Approved by:


Major Professor

**THIS BOOK
CONTAINS
NUMEROUS PAGES
WITH THE ORIGINAL
PRINTING BEING
SKEWED
DIFFERENTLY FROM
THE TOP OF THE
PAGE TO THE
BOTTOM.**

**THIS IS AS RECEIVED
FROM THE
CUSTOMER.**

Document
LD
2668
T4
1977
W53
C. 2

TABLE OF CONTENTS

	Page
Table of Contents	i
List of Figures	ii
List of Tables	iv
Acknowledgements	v
Chapter I: INTRODUCTION	1
Chapter II: THEORETICAL CONSIDERATIONS	5
a. Simulations	5
b. Parameters	13
Chapter III: EXPERIMENTAL PROCEDURE	20
a. Beam and Chamber	20
b. Observation of the Mössbauer Spectrum	24
Chapter IV: DATA AND ANALYSIS	28
Chapter V: CONCLUSIONS	46
Appendix: The Program MOSFIT	51
Notes	64
Bibliography	65
Abstract	69

LIST OF FIGURES

- Figure 1. (a) Split interstitial in a face-centered cubic lattice.
(b) Simplified collision sequence. The primary knock-on leaves a vacancy at A; it starts side chains at B and C - the chain started at B is a matter/energy chain, and a vacancy is left at B, while the chain started at C transmits energy only; replacements occur at D and E; finally the chain ends with the formation of a split interstitial at F.
- Figure II. Classical excitation functions for E2 excitations as a function of the dimensionless parameter, . This is Figure II.5 from Alder, Bohr, Huus, Mottelson, and Winther (p.460).
- Figure III. Diagram of the target chamber, showing the configuration in which it was used: The cold finger, which extends from the bottom of the chamber, has its upper end cut away (as shown in the upper detail) to allow mounting the target; the absorber mount (lower detail) is attached to the ends of the four rods shown in the drawing of the chamber.
- Figure IV. Collection Circuit. The circuit used to take all the source spectra (those made with radioactive sources) is identical, except that a proportional counter - biased at +2200 volts - was used; the linear gate and pulse-height analyzer were not used for these spectra.

Figure V. Source - $^{57}\text{Co}(\text{S.S.})$; Absorber - new S.S. foil.

Figure VI. Source - $^{57}\text{Fe}(\text{p,p})^{57}\text{Fe}$; Absorber - ferrocyanide.

Figure VII. Source - $^{57}\text{Co}(\text{Pd})$; Absorber - irradiated foil.

Figure VIII. Source - $^{57}\text{Co}(\text{Pd})$; Absorber - annealed foil.

Figure IX. Source - $^{57}\text{Co}(\text{S.S.})$; Absorber - ferrocyanide.

Figure X. Source - $^{57}\text{Co}(\text{Pd})$; Absorber - ferrocyanide.

Figure XI. Horizontal axis is channel number (or energy), vertical axis is counts per channel.

(a) Segment of the spectrum of 5.0 MeV protons on stainless steel; no shielding foil was used. The large peak is the Fe K x-ray doubling peak.

(b) The same spectrum as (a), except that a .5 mil chromium foil was placed between the target and the detector.

(c) The same spectrum as (a) and (b), but using a 2.0 mil chromium foil as a shield.

(d) Segment of the spectrum from a $^{57}\text{Co}(\text{Pd})$ source, showing the location of the 14.4 keV gamma peak.

Spectra (a), (b), and (c) all were made with the same beam current and exposure time.

LIST OF TABLES

Table I. Values of the classical excitation function and cross-section for electric quadrupole coulomb excitation for selected energies.

Table II(a). Catalogue of spectra analyzed.

(b). Parameters of these spectra, as determined by MOSFIT (best fit).

Table III. Form of the isomer shifts from Table II.

Table IV. Isomer shifts for the stainless steel foil at various times.

ACKNOWLEDGEMENTS

The subject of this investigation was brought to my attention by John Eck; as my major professor, he provided continual assistance and guidance, in many ways. He suggested or demonstrated procedures followed, and made certain that all necessary operations were carried out and that all required data was collected. The assistance of other members of the physics faculty and staff must be recognized: R. D. Dragsdorf, for much advice on solid-state aspects of the investigation; James H. McGuire for assistance in understanding the theory of Coulomb excitation; Basil Curnutte, for answering some questions about inner-shell electron excitations and their lifetimes; and David Hill, of the Instrument Shop, for helping me design the target chamber and for building it so quickly.

Other assistance than that directly relating to the investigation was also provided at times. Specifically, I wish to acknowledge the support of my family and friends; I am very grateful for their support and encouragement during the difficult moments of the study.

Finally, the financial support provided by the Energy Research and Development Administration in the form of various grants must be recognized. Without this support, the investigation could never have been conducted.

INTRODUCTION

The damage to stainless steel resulting from bombardment with atomic and subatomic particles - particularly neutrons - is a matter of considerable practical interest, as such damage to the coolant pipes and other steel constructions around reactor installations could result in hazardous conditions and necessitates periodic replacement of these components.¹ For instance, the result of ignoring the cumulative damage to the stainless steel in the coolant pipes of a fission reactor could conceivably be a massive coolant failure and resultant core melt-down. The problem of radiation damage to crystalline materials is complex and includes many lines of research; this study deals with one aspect of the problem - the nature of the damage occurring immediately after a particle collides with a stainless steel lattice - and investigates the feasibility of using the Mössbauer effect following Coulomb excitation for studying such damage. Later work may eventually lead to the discovery of ways to treat steels which will be exposed to high particle fluxes so that they will be less susceptible to damage.

A common technique for studying damage to crystalline substances caused by particle bombardment involves exposing the material under study to a high flux of the desired particles, then removing the material from the flux and studying the damage to its structure by means of x-ray crystallography. This method is very useful for studying the permanent or long-term damage; as it requires a considerable delay between the occurrence of the initial damage and study of the damage, it is not satisfactory for examining processes occurring immediately after the bombarding particle

strikes the lattice. During the delay, the original damage may be modified or may anneal out of the crystal. To avoid this difficulty, a technique must be used which allows bombardment and study to occur at the same time.

The Mössbauer effect following Coulomb excitation allows observation of the lattice structure around certain atoms within a very short interval of time after these atoms have taken part in a damage-causing event. To study neutron-induced damage by this technique, the effects of neutron bombardment are simulated by proton bombardment. As the projectile masses are essentially the same, the damage from kinetic energy transfer to atoms in the target caused by the protons should be a reasonable approximation of that caused by neutrons.

The process begins when an accelerated proton strikes the stainless steel foil; it engages in a series of collisions with the atoms in the foil, transferring at each collision a certain amount of kinetic energy. If the energy transferred to the struck atom - the "primary knock-on" - is greater than a threshold amount (of the order of 20 to 80 electron volts (eV)), this atom will leave its original lattice site; a vacancy remains at this site, while the displaced atom moves through the crystal until its energy is dissipated. This process is the object of the investigation.

The accelerated proton carries one unit of electric charge, and the electric and magnetic fields associated with this moving charge are capable of interacting with the charged nucleus, transferring energy to its internal coordinates and thereby raising it to an excited energy state. Following this "Coulomb excitation", the nucleus de-excites by emitting gamma rays, electron and x-rays, or a combination of these. If the excited atom is located in a crystal, part of the energy given up by

de-excitation is usually dissipated as lattice recoil. However certain isotopes, when bound in crystals, will frequently de-excite from low-lying states without recoiling. This recoilless - or Mössbauer - emission is the basis of the method used to investigate the damage.

The nuclear excited states which are useful for Mössbauer spectroscopy decay by emission of a γ ray; for these particular γ -ray emissions, a significant percentage of the radiation carries energy exactly equal to the energy difference of the two nuclear levels. Thus, the energy of the photon may be known quite precisely. The crystal environment around the emitting nucleus can modify the electric and magnetic fields at that nucleus, as well as the electron density at the nucleus. These modifications may then affect the energy of the emitted radiation; careful observation of the energy spectrum can yield information about the kind of lattice environment in which the Coulomb-excited nucleus is located when it de-excites. As this atom will have taken part in the damage process, the spectrum may, in turn, provide information about the nature of the damage.

There are two isotopes suitable for use in such studies which can be incorporated into stainless steel - ^{57}Fe and ^{61}Ni .² In this work, stainless steel foils have been used which have been 91% enriched with ^{57}Fe ; the long half-life for the excited state of this isotope (98 nanoseconds) allows the atom to come to rest before the nucleus de-excites. The half-life is also sufficiently long for disturbances of the inner shell electrons to equilibrate,³ thereby removing one complicating factor from the final spectrum. This isotope has been widely used in Mössbauer studies of various types, so the behavior of its spectrum is well known.

One Mössbauer study of particular interest to this investigation was published by a group at Johns Hopkins University in 1965.⁴ This group used a beam of α -particles to damage and Coulomb-excite a target foil composed of α -iron, enriched with ⁵⁷Fe. The usefulness of such studies in a more complicated lattice will be investigated and information which may be obtained about the damaged lattice using this technique will be studied.

THEORETICAL CONSIDERATIONS

As the preceding chapter describes, this investigation involves the use of a beam of accelerated protons to simulate neutron-induced radiation damage in a stainless steel target foil; this foil is 91% enriched with ^{57}Fe . The protons also Coulomb-excite the ^{57}Fe nucleus, primarily to the second excited state at 136 keV. This state predominately decays to the first excited state at 14.4 keV; it is the de-excitation of this state which yields the γ -ray studied by Mössbauer spectroscopy.

In the following sections of this chapter, a simulation of the radiation-damage process will be described, with its assumptions and predictions, and the theory used to determine the parameters of the experiment will be discussed.

a. Simulations

In the first half of the 1960's, G. H. Vineyard and various colleagues at the Brookhaven National Laboratory published a series of papers on radiation damage in FCC⁵ and BCC^{6,7} crystals. All three papers were based on computer simulations. The general procedure was to take a set of 500 to 1000 atoms in a crystal lattice which was initially perfect. These atoms interact with fairly realistic forces; in order to treat this "microcrystallite" as part of an infinite crystal, extra forces are applied to atoms on the edges and faces of the set. To start a radiation damage event, one atom (the "primary knock-on") suddenly acquires momentum from some unspecified source. By solving the classical equations of motion for all atoms in the set, the course of the damage process and the final state of the microcrystallite may be determined. Annealing of damage may also be studied in this manner, starting with the damaged crystal and following its behavior in time.

The specific cases studied were copper (FCC) and α -iron (BCC). The system under investigation in this study is Type 310 stainless steel. This type is austenitic, and hence FCC.⁸ Its composition is:⁹

Cr	24-26%	Si	$\leq 1.50\%$	S	$\leq 0.030\%$
Ni	19-22%	C	$\leq 0.25\%$	Fe	remainder
Mn	$\leq 2.00\%$	P	$\leq 0.04\%$		

(For most purposes, it is sufficient to list the composition as 55% Fe, 25% Cr, and 20% Ni, ignoring the minor constituents.) Due to the difference in type of atom, the various constants of the crystal (lattice parameter, bulk modulus, and so on) will differ from the values given in the papers cited above,⁵⁻⁷ but the general discussion for a FCC lattice should still apply.

To allow the carrying out of the calculations described with available computers and in reasonable time, certain assumptions and approximations had to be made. In the first place, all calculations were carried out at absolute zero; the thermal effects could in principle be allowed for by giving the atoms small agitations about their lattice sites, but this would greatly increase the amount of calculation necessary.

An important approximation is that the boundary forces used - a combination of spring and viscous forces - are adequate to give the effect of embedding the microcrystallite in an infinite perfect crystal. As these boundary forces are a first-order approximation, it was not desirable for a damage chain to reach the microcrystallite boundary and to cause large displacements of the boundary atoms. This restriction limits the range of initial energies available.

The other major approximation is the interatomic potential used, for the FCC paper, a Born-Mayer potential was used, of the form:

$$\phi(r) = A \exp(-\rho(r - r_0)/r_0), \quad (1)$$

where r_0 is the nearest-neighbor distance at zero pressure and 0°K., and A and ρ are parameters chosen to give the correct threshold energy for production of permanent displacements. This potential, with reasonable allowance for contributions from the conduction electrons and from interaction of the ions with the conduction electrons, yields values for the elastic moduli in good agreement with experimental values.¹⁰ However, these electronic corrections are not contained in the model. The authors estimate that this omission should not appreciably affect the dynamic parts of the simulation, but that the stability of lattice defects may be incorrectly evaluated. (It should be noted that a more complex potential was used in the papers on BCC α -iron, but the results were qualitatively similar.)

The simulation on a FCC copper lattice considers primary knock-ons with initial energies in the range 20-400 eV and with a variety of initial directions. As the energy range in this experiment is much wider - 0 to 350 keV - careful extension of the results reported is required. This will be done in accordance with the findings of Vineyard, et al., with the extension of their low and medium-energy calculation for a BCC lattice⁶ to energies as high as 1500 eV.⁷ In other words, the type and amount of damage are assumed to change in the same way with increasing energy for BCC and FCC lattices.

In all cases for which the initial energy was sufficiently high to cause any damage, the primary knock-on left a vacancy at its initial lattice site and moved a distance determined by its initial energy and direction,

then made a replacement collision with another lattice atom; if its energy was high enough, the primary knock-on could transmit appreciable amounts of kinetic energy to other atoms in glancing collisions before it stopped. The atom replaced and any side chains continue the process of replacement until the kinetic energy becomes too low to permit further replacement (≤ 3.5 eV in Cu). At this point, a split interstitial is formed; this occurs when two atoms try to occupy the same lattice site. The resulting configuration has both atoms displaced off the lattice site on opposite sides; the amount of the displacement is less than one-half the lattice parameters. (Fig. I(a)).

Besides the chains which transmit matter and energy, there are chains which transmit only energy. These are chains in which the atoms receive enough energy to strongly perturb them from their normal lattice sites, causing them to perturb other atoms. The energy received, however, is not enough to allow displacement; these atoms eventually relax back into their initial positions. Such a chain is shown in Figure I(b).

Both the threshold energy and the rate of energy loss (and, thus, the length of the collision chains) are highly dependent on the direction of the initial momentum. In this experiment, however, crystal orientation is not a known factor; therefore, the predictions of the theory in this area cannot be checked, and little purpose would be served by detailing them here.

A Frenkel pair is composed of an interstitial and the associated vacancy. The minimum distance by which these must be separated in order for the pair to be stable varies with direction, but in general if the vacancy and interstitial are no closer than fourth-nearest neighbors on

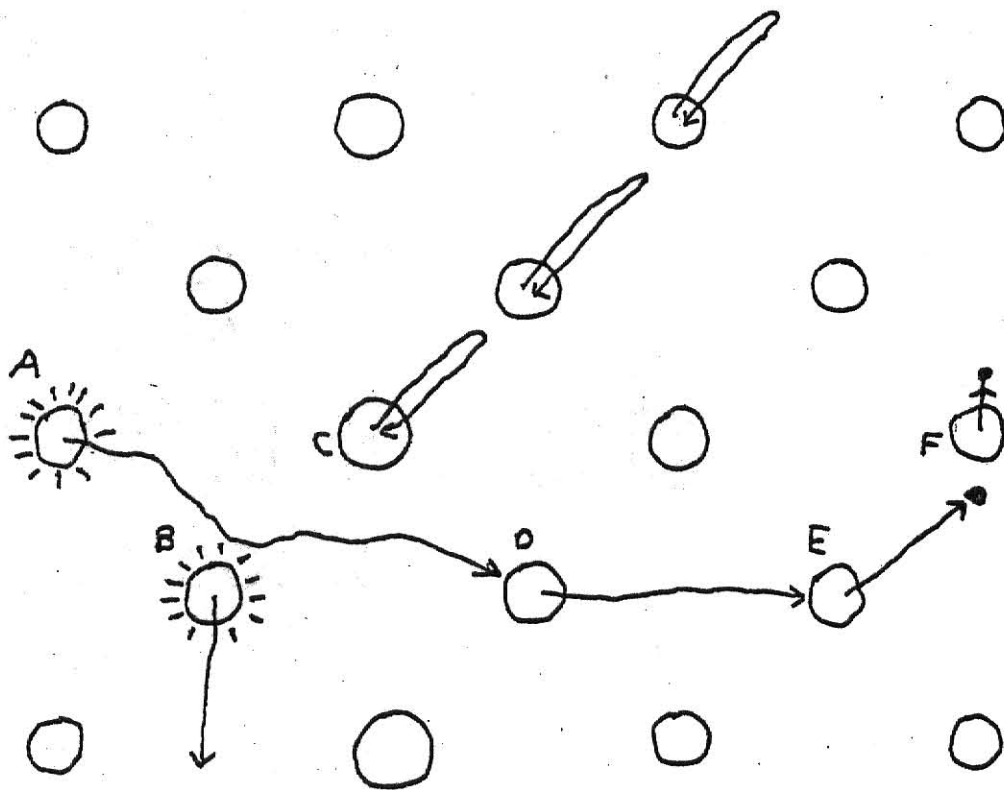
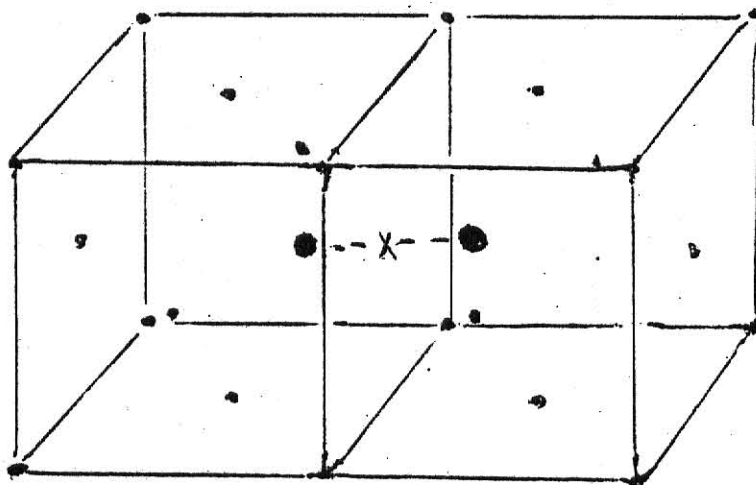
**THIS BOOK
CONTAINS
NUMEROUS PAGES
THAT WERE
BOUND WITHOUT
PAGE NUMBERS.**

**THIS IS AS
RECEIVED FROM
CUSTOMER.**

- Figure I. (a) Split interstitial in a face-centered cubic lattice.
- (b) Simplified collision sequence. The primary knock-on leaves a vacancy at A; it starts side chains at B and C - the chain started at B is a matter/energy chain, and a vacancy is left at B, while the chain started at C transmits energy only; replacements occur at D and E; finally the chain ends with the formation of a split interstitial at F.

**THIS BOOK
CONTAINS
NUMEROUS PAGES
WITH DIAGRAMS
THAT ARE CROOKED
COMPARED TO THE
REST OF THE
INFORMATION ON
THE PAGE.**

**THIS IS AS
RECEIVED FROM
CUSTOMER.**



the line containing them both, the pair will be stable and will not spontaneously anneal. The number of such pairs produced increases with the energy of the primary knock-on; at 100 eV, at least one pair will be produced, while at 400 eV as many as eleven pairs may be produced (depending on the initial energy). In the 1965 paper, the authors found that the number of Frenkel pairs produced at energies up to 1500 eV approximately follows the relation:

$$N_d = E/C, \quad (2)$$

where C varies with direction but not with energy; E is the initial energy of the primary knock-on. It seems reasonable that the number of defects produced as a function of energy (for any given direction of initial momentum) has a similar form for a FCC lattice, but the value of the constant, C , is unknown for this situation. All that can be said is that the number of Frenkel pairs produced for any fixed direction of primary knock-on initial momentum may be a linear function of primary knock-on initial kinetic energy.

It should be noted that all the vacancies produced in any one radiation-damage event remain clustered near the original site of the primary knock-on, while the interstitials are more dispersed and are found at a distance from this site. The configuration of the vacancies may change spontaneously, but no evidence was found (in these simulations) for the formation of any kind of defects except split interstitials and vacancy clusters at energies up to 1500 eV.

To compliment this discussion of the theoretical damage process, a consideration of the information about the crystal contained in the Mössbauer spectrum would be helpful.

Without going into the details of interpretation of Mössbauer spectra, there are four features of a spectrum which can yield information about the lattice neighborhood in which the excited nucleus is located when it emits the radiation being studied: (1) magnetic hyperfine splitting; (2) electric quadrupole splitting; (3) isomer shift; and (4) line width. The first of these magnetic hyperfine splitting, gives information about the magnetic fields experienced by the emitting nucleus. As the material under study is stainless steel, which has no permanent internal magnetic field, and as no external fields are being applied, no hyperfine splitting is expected.

The second feature, electric quadrupole splitting, is caused by the interaction of the electric quadrupole moment of the emitting nucleus with the electric field gradient at that nucleus; this field is caused by other ions in the lattice, electrons in the materials, and possibly the electrons belonging to the emitting atom (due to perturbations to the shells caused by the other fields). The electric field gradient vanishes at a cubic lattice site, as there are mutually perpendicular three-fold axes of symmetry intersecting at such a point¹¹; if the primary knock-on (which is also the excited nucleus) ends up on a lattice site, as the theory predicts, there should be no appreciable splitting unless the crystal is so heavily damaged that there are vacancies or interstitials in the immediate neighborhood.

The isomer shift is a function of the radius of the emitting nucleus in the excited and ground states, and also the density of electrons at the nuclei of the emitting and absorbing atoms. The emitting atom will always be ^{57}Fe , so the radius-dependent part of the shift should be constant; the absorbing nucleus will also be ^{57}Fe , but both emitting and absorbing

atoms may be located in a variety of molecular or crystalline environments in the different spectra. Therefore, the electron-density-dependent term, which involves both the source and the absorber, will not be constant.

Broadening of a spectral line may be due to several causes. It may be caused by thermal motion of the emitting atom, which Doppler-shifts the energy of the radiation from that nucleus. It may be due to an unresolved electric quadrupole splitting, where the splitting is too small for the apparatus to separate. Finally, line broadening may be the result of superposition of a number of lines with slightly differing isomer shifts. This would be the result of varying electron densities at the source or absorber nucleus. As an example of the last named cause of broadening, a spectrum taken with a ^{57}Co source in a stainless steel matrix always shows a broader line than one taken with a source which has ^{57}Co in a palladium matrix; this is because the stainless steel source may have a variety of possible neighborhoods around the Co atom, while the neighborhood of a Co atom in palladium is always the same. The neighboring atoms have an effect on the electron density at the nucleus, so the stainless steel source will display a variety of isomer shifts, rather than a single shift. As a result, the line emitted by the stainless steel source will be broader.

b. Parameters

In order to obtain the best spectrum possible in a reasonable length of time, it was necessary to calculate some factors in the design of the experiment prior to attempting to collect data. Of these, the most important was the energy dependence of the cross-section for Coulomb excitation of the ^{57}Fe nucleus by protons. Some attention had to be paid also to the

amount of heating of the target foil caused by various beam currents.

These matters will be considered in that order.

In the calculations to determine the best beam energy to use for this experiment, the development presented by K. Alder, et al.,¹² was used; this paper presents the classical and quantum mechanical theory of electromagnetic excitation of nuclei by accelerated ions. Based on this development, the total cross-section for an electric excitation of multipole order, λ , is:

$$\sigma_{E\lambda} = c_{E\lambda} E_{\text{MeV}}^{\lambda-2} (E_{\text{MeV}} - \Delta E'_{\text{MeV}})^{\lambda-1} B(E\lambda) f_{E\lambda}(\eta_1, \xi) \quad (3)$$

$$\text{where } c_E = (Z_1^2 A_1 / 40.03) (0.07199(1 + A_1/A_2) Z_1 Z_2)^{-2} + 2 \text{ barns}$$

$$E_{\text{MeV}} = \text{initial energy of the projectile (lab)}$$

$$\Delta E'_{\text{MeV}} = (1 + A_1/A_2) \Delta E, \text{ with } \Delta E = \text{excitation energy}$$

$$B(E\lambda) = \text{reduced transition probability associated with a radiative transition of multiple order (measured in units of } e^2 (10^{-24} \text{ cm}^2) \text{).}$$

$$f_{E\lambda}(\eta_1, \xi) = \text{excitation functions (tabulated in paper), where}$$

$$\eta_1 = (Z_1 Z_2 / 2) (A_1 / 10.008 (E_{\text{MeV}}))^{1/2} \text{ (dimensionless)}$$

$$\xi = (Z_1 Z_2 e^2 / hV) (\Delta E / 2E) \text{ (dimensionless)}$$

(In the preceding, '1' refers to the projectile; Z is atomic number, A is mass number, and V is the velocity of the projectile.) In the classical treatment, the excitation function is a function of ξ only; η_1 goes to ∞ as a limit.

There is a similar expression for magnetic transitions; however, any magnetic excitation has a cross-section smaller than the corresponding electric excitation by a factor of the order of $(v/c)^2$, apart from differences in the nuclear matrix elements. For 5.0 MeV protons, this is of the order of 0.01. Thus, the magnetic transitions can generally be ignored.

The particular excitation of interest in this experiment is that from the ground state of ^{57}Fe to the 136 keV second excited state; this is an electric quadrupole transition (E2). In formula (3), c_{E2} and $B(E2)$ are constants with respect to energy of the projectile, while $(E_{\text{MeV}} - \Delta E'_{\text{MeV}})$ is a linear function of energy. Figure II shows that the classical excitation function, $f(\xi)$, is a monotone-decreasing function of ξ in the range (0, 1.4); $\log f_{E2}(\xi)$ is an approximately linear function of ξ with negative slope. As ξ is proportional to $E^{-3/2}$, it is seen that $\log f_{E2}(E)$ is a monotone-increasing function of energy. In general, therefore, the cross-section for electric quadrupole excitation of ^{57}Fe nuclei by protons is a monotone-increasing function of projectile energy which increases faster than a linear function of slope, 1, in the energy range 300 keV to 10 MeV.

To illustrate this, the following cross-sections are calculated, using the classical excitation functions from Table II.3 of the paper:

TABLE I

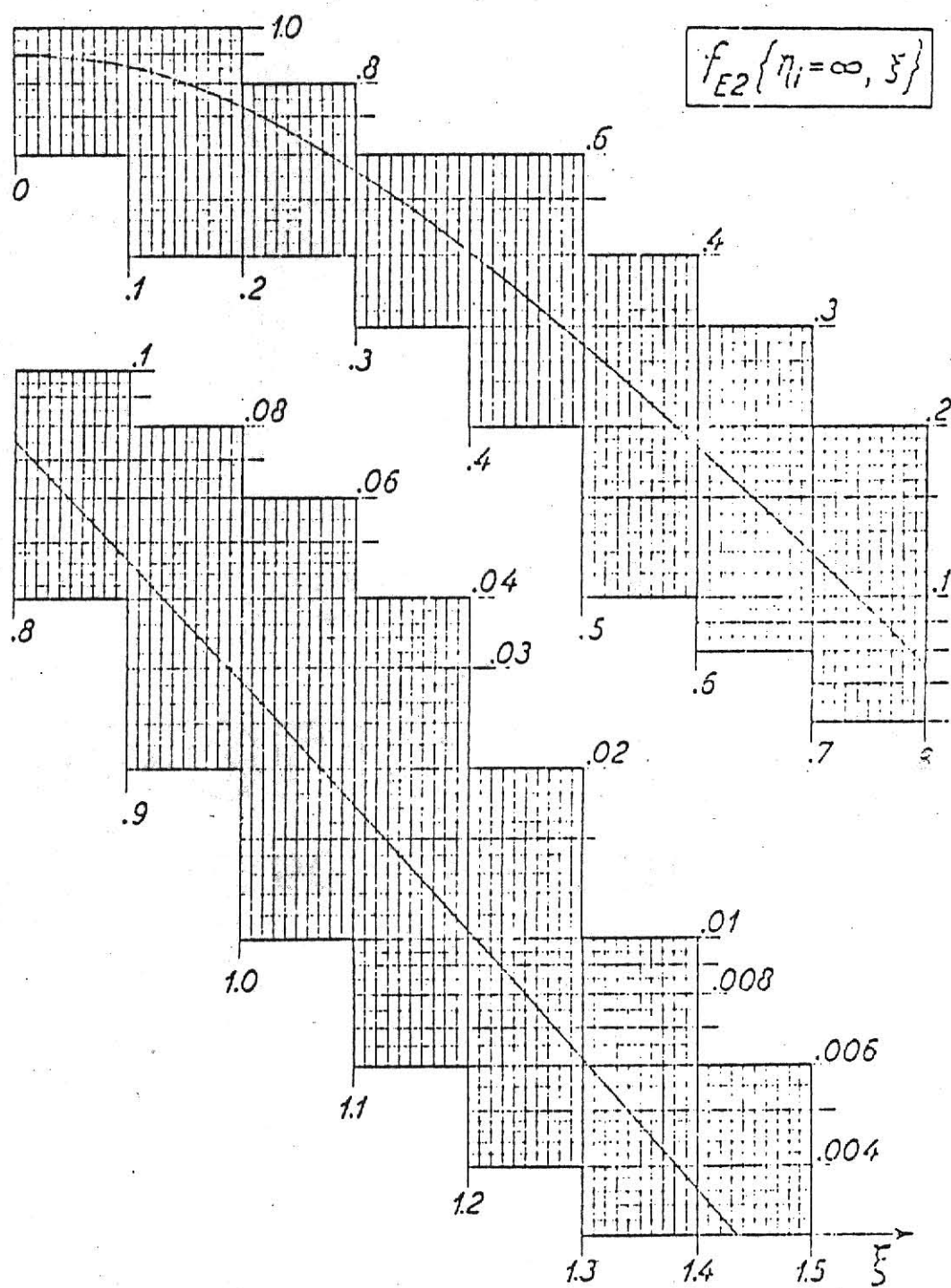
E_{lab}	$E_{\text{c.m.}}$	$f_{E2}(\xi)$	σ_{E2}
1.5 MeV	1.45 MeV	.778	.352 millibarns
5.0	4.83	.885	1.43
6.7	6.49	.889	1.94

Figure II. Classical excitation functions for E2 excitations as a function of the dimensionless parameter, η . This is Figure II.5 from Alder, Bohr, Huus, Mottelson, and Winther (p. 460).

ILLEGIBLE DOCUMENT

**THE FOLLOWING
DOCUMENT(S) IS OF
POOR LEGIBILITY IN
THE ORIGINAL**

**THIS IS THE BEST
COPY AVAILABLE**



In order to maximize the number of excited nuclei, the projectile energy should be made as large as possible. However, there is an upper limit to the energy which can be used. Of necessity, a large amount of aluminum is used in the target chamber (see Chapter III); the (p,n) threshold of aluminum is about 5.5 MeV. When protons with higher energies than this strike an aluminum object, the ensuing reaction releases large numbers of neutrons; this neutron burst is extremely harmful to semiconductor detectors (such as the Si(Li) detector which was used for this experiment). To maximize the excitation cross-section while remaining safely below the aluminum (p,n) threshold, it was decided to use a projectile energy of 5.0 MeV.

To estimate the thermal gradient maintained between the beam spot and the edge of the foil, it was necessary to make several assumptions. Using the one-dimensional heat-flow equation:

$$q = -kA \, dT/dr \quad (4)$$

in the integrated form appropriate to a plane polar geometry:

$$q = 2 \, tk \, (T_1 - T_2) / \ln (r_2/r_1), \quad (5)$$

with t being the target thickness, k the thermal conductivity of the foil, q the rate of heat flow, T the temperature and r the radius, and 1 and 2 referring to the beam spot and target frame respectively. Equation (5) assumes that the beam spot and target frame are concentric circles.

This is obviously an approximation, since the target being mounted at 45° to the beam axis causes the actual beam spot to be an ellipse. Furthermore, the beam and the target frame are not necessarily concentric.

The value of the thermal conductivity of Type 310 stainless steel is also approximate.

The value of the rate of heat flow, q , can be set equal to the rate of heat input in an equilibrium situation. This can be calculated as a function of beam current, using range tables¹³ to estimate the energy lost by a proton in the foil. Doing this and using the approximations mentioned yields an estimate of the thermal gradient maintained by a beam of 5.0 MeV proton in a stainless steel foil of approximately $.1^{\circ}\text{C}$ at a beam current of 30 nanoamps.

As the temperature at the edge of the foil, T_2 , is approximately the ambient temperature (293°K), it is clear that the amount of heating to be expected with a beam current of 30 nanoamps - the current which was used - is completely negligible. There should be no significant thermal shift of the gamma energy. If the Debye temperature of a stainless steel lattice is approximated by that of iron (440°K), it is clear that the recoilless fraction, f , is not significantly changed by this temperature difference.¹⁴

As a result of these calculations, the experiment was performed with a 30 nanoamp beam of 5.0 MeV protons.

EXPERIMENTAL PROCEDURE

The experiment involved irradiating a target foil of Type 310 stainless steel with protons while simultaneously observing the spectrum of scattered and emitted radiation, isolating the 14.4 keV gamma ray emitted by the ^{57}Fe nucleus, and collecting a Mössbauer spectrum of that line. The apparatus and procedures can be discussed in two sections: (a) beam and chamber; and (b) observation of the Mössbauer spectrum. Each will be described in detail.

a. Beam and Chamber

As described in Chapter II(b), it was decided to use a beam of 5.0 MeV protons for irradiation, with a beam current of about 30 nanoamps. (Current actually varied from 10 to 40 nanoamps indicated on target.) This beam was obtained from the EN Tandem Van de Graaff accelerator at Kansas State University, using the diode ion source.

Two tantalum collimators, 15 cm apart and with round apertures of radius, .24 cm were used to define the beam and to assure that it was centered on the stainless steel target and not striking other components which might give rise to undesirable background radiation. These collimators were located approximately 1.25 m ahead of the chamber in the beam line.

As the radiation of interest in this experiment is the 14.4 keV γ -ray from the first excited state of ^{57}Fe which is bound in a stainless steel lattice, this peak tends to be obscured by the iron and nickel atomic x-ray peaks. To avoid making the Mössbauer spectrum any more difficult to observe, it was necessary that there be no

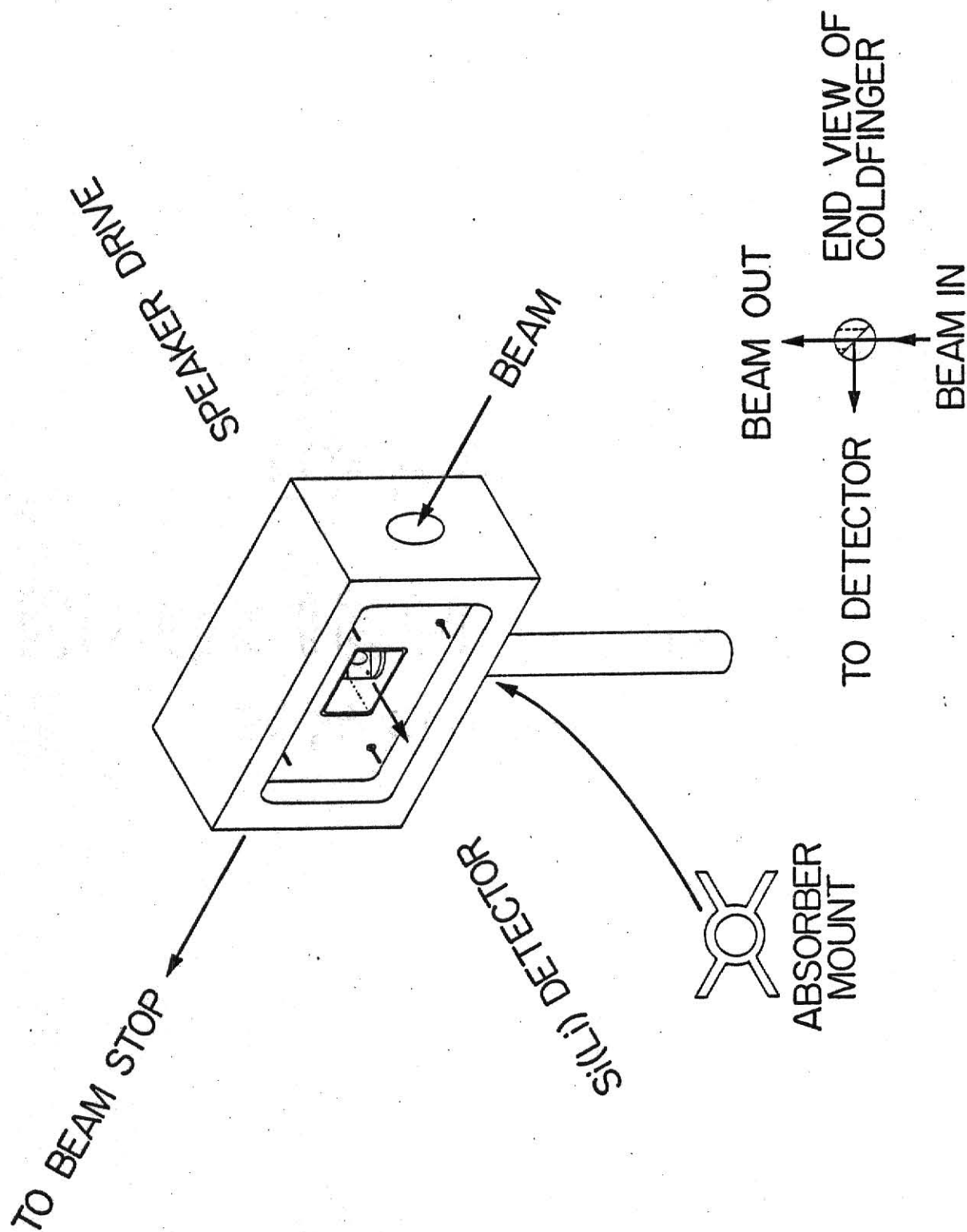
other iron or steel near the target; protons scattered in the target could cause additional background radiation from other steel objects, and the 14.4 keV gamma radiation could cause fluorescence of Cr, Fe, or Ni in steel.

Therefore the chamber itself and all beam line components after the chamber are made principally of aluminum (whose atomic x-rays are of very low energy); the other materials used are nylon and Lucite. The chamber is symmetric with respect to its sides and ends, and has viewing quartzes at both ends; the target is mounted on an aluminum cold finger. This apparatus may be adapted to almost any configuration of loudspeaker drive and detector. The chamber has four holes drilled in it to accommodate a cage, by means of which the speaker drive - mounted on one side of the chamber - can oscillate an absorber between the target and the detector on the opposite side of the chamber (Fig. III).

Each of the cold fingers prepared for use with this chamber has a hole drilled through it to allow protons to continue down the beam line unimpeded after passing through the target foil. Each cold finger is cut away at the top in such a way that the target foil is mounted at a 45° to both the incoming beam and the target-detector line. The aluminum target frame is attached to the cold finger with two nylon screws.

After the beam passes through the target, it leaves the chamber and is stopped in the following 1.37 m of aluminum beam pipe or in the aluminum blank-off at the end. The blank-off and the last 15 cm of beam pipe are electrically insulated from the rest of the beam line, and could potentially be used as a Faraday cup to measure beam current. (This was not done; beam current was measured on the cold finger, which is also electrically

Figure III. Diagram of the target chamber, showing the configuration in which it was used: The cold finger, which extends from the bottom of the chamber, has its upper end cut away (as shown in the upper detail) to allow mounting the target; the absorber mount (lower detail) is attached to the ends of the four rods shown in the drawing of the chamber.



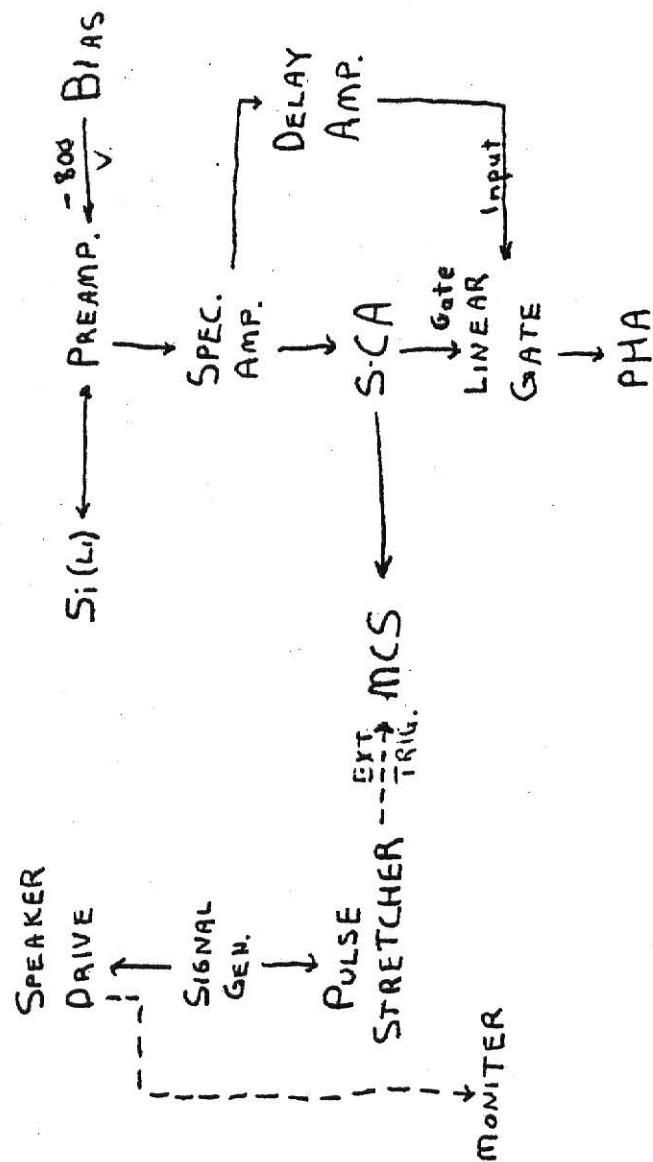
insulated from the beam line - these readings agreed reasonably well with those obtained at a built-in Faraday cup 50 cm before the chamber.)

b. Observation of the Mossbauer Spectrum

A series of preliminary observations of energy spectra, taken with various beams in a different scattering chamber, showed that a Si(Li) detector was able to resolve the 14.4 keV peak from the background due to the Fe and Ni atomic x-rays when aluminum foil was used as a shield in front of the detector window. The optimal foil thickness was about .15 mm. Spectra taken without the foil showed no sign of the 14.4 keV peak; it was buried in the trailing edge of a peak at 12.8 keV - that peak was the result of the extremely high rate of Fe x-ray production, which caused doubling in the detector. By the use of coincidence circuitry, which has been used previously, it is possible to separate the 14.4 keV peak from the background radiation, however, the use of Al shielding to reduce the amount of lower-energy radiation reaching the detector makes it possible to resolve the peak in the energy spectrum without the need for a coincidence.

No Al foil was used for the Mössbauer spectrum; it is determined that the disc of ^{57}Fe -enriched $\text{NaFe}_2(\text{CN})_6 \cdot 10 \text{H}_2\text{O}$, embedded in a Lucite disc, used as a Mössbauer absorber gave the same shielding effect at the optimum thickness of aluminum foil. The 14.4 keV peak was clearly visible on the high-energy side of the doubling peak. To take the Mössbauer spectrum, a single-channel analyzer (SCA) window was set on this peak, and the output of the SCA was collected in a multichannel analyzer (MCS) operating in the time mode. The Start signal for the multiscaling mode

Figure IV. Collection Circuit. The circuit used to take all the source spectra (those made with radioactive sources) is identical, except that a proportional counter - biased at +2200 volts - was used; the linear gate and pulse-height analyzer were not used for these spectra.



was synchronized with the velocity waveform. (The circuits used allowed gating the SCA out of the circuit if it was desirable to examine the energy spectrum in a pulse-height analyzer (PHA)).

The speaker drive was operated in the constant acceleration mode; it was driven by a triangular wave from a single generator. Calibration spectra were taken before and after the irradiation run, using a $^{57}\text{Co(Pd)}$ source - ^{57}Co embedded in a palladium matrix - and an enriched (with ^{57}Fe) iron foil. The velocity waveform was frequently checked from a feedback connection on the drive with an oscilloscope. It showed no distortion before or during the irradiation run; however, a spectrum was taken immediately after the irradiation run, using a source and using the irradiated stainless steel foil as an absorber. (The unirradiated area was masked with one of the tantalum collimators.) During the collection of this spectrum, the velocity waveform began to show serious distortion, indicating that the cage bars were rubbing against the sides of the holes through which they run between the speaker drive and the absorber mount. The spectrum was so distorted that it was useless. The spectrum of the irradiated foil actually used in the analysis was collected starting about 18 hours after the end of the irradiation, the foil being kept at room temperature during this period.

Total irradiation time was $85 \pm .25$ hours, spread over four days; this includes only that time during which the beam was irradiating the foil and the Mössbauer spectrum was accumulating.

The other spectra were taken with the apparatus on a laboratory bench, using the indicated radioactive source and using a proportional counter (PC) as a detector.

DATA AND ANALYSIS

In addition to the spectrum taken during the irradiation of the target foil, a number of spectra were taken using radioactive sources - ^{57}Co in a palladium or stainless steel matrix - in order to facilitate the comparison of that spectrum with spectra of the same foil made before and after irradiation. The spectra used are listed in Table II(a).

The spectrum collected in the MCS is made up of two mirror-image spectra, one collected when the speaker drive has positive acceleration and the other when it has negative acceleration. Before use, this spectrum must be folded into a single spectrum. The folding of all spectra used was performed with the program MBRFLD, written for a PDP-8 computer by K. F. Purcell of the Chemistry Department at Kansas State University. The folded spectra were fitted by one or more Lorentzians of arbitrary position, width, and depth superimposed on an arbitrary background. These fits were calculated and plotted by an IBM 370 computer, using the program MOSFIT (see Appendix). Each spectrum was fitted at least twice, using different sets of initial values of the fitting parameters to verify that the final "best-fit" values were the same. In all cases, the final values of the parameters agreed to at least four significant figures. The background, isomer shift, and linewidth for each spectrum are listed in Table II(b). The data points and the fitted spectra are shown in Figures V - X.

The isomer shifts in Table II(b) are with respect to a zero-velocity channel and a velocity/channel conversion determined from a calibration spectrum made with the same source and a 91% enriched iron foil. The

TABLE II (a)

No.	Source	Absorber	Figure
1	^{57}Co in S.S. matrix	new enriched S.S. foil	V
2	$^{57}\text{Fe}(\text{p,p})$ $^{57}\text{Fe}^*$	enriched $\text{NaFe}_2(\text{CN})_6$	VI
3	^{57}Co in Pd matrix	irradiated S.S. foil spectrum 2, with unirrad. area masked by Ta collimator	VII
4	^{57}Co in Pd matrix	same foil after annealing at 394 K. for about 150 min.	VIII
5	^{57}Co in S.S. matrix	enriched $\text{NaFe}_2(\text{CN})_6$	IX
6	^{57}Co in Pd matrix	enriched $\text{NaFe}_2(\text{CN})_6$	X

(In all cases above, S.S. is type 310 stainless steel)

TABLE II (b)

No.	Background (counts)	Isomer Shift (mm/sec)	Width (mm/sec)
1	401947 \pm 123	0.094 \pm .004	0.443 \pm .066
2	164660 \pm 111	0.016 \pm .041	0.519 \pm .082
3	405837 \pm 776	0.089 \pm .002	0.338 \pm .004
4	280255 \pm 366	0.105 \pm .002	0.345 \pm .004
5	108087 \pm 122	0.077 \pm .002	0.338 \pm .003
6	151498 \pm 162	0.092 \pm .001	0.327 \pm .003

(The ranges listed above are \pm one standard deviation.)

Figure V. Source - $^{57}\text{Co}(\text{S.S.})$; Absorber - new S.S. foil.

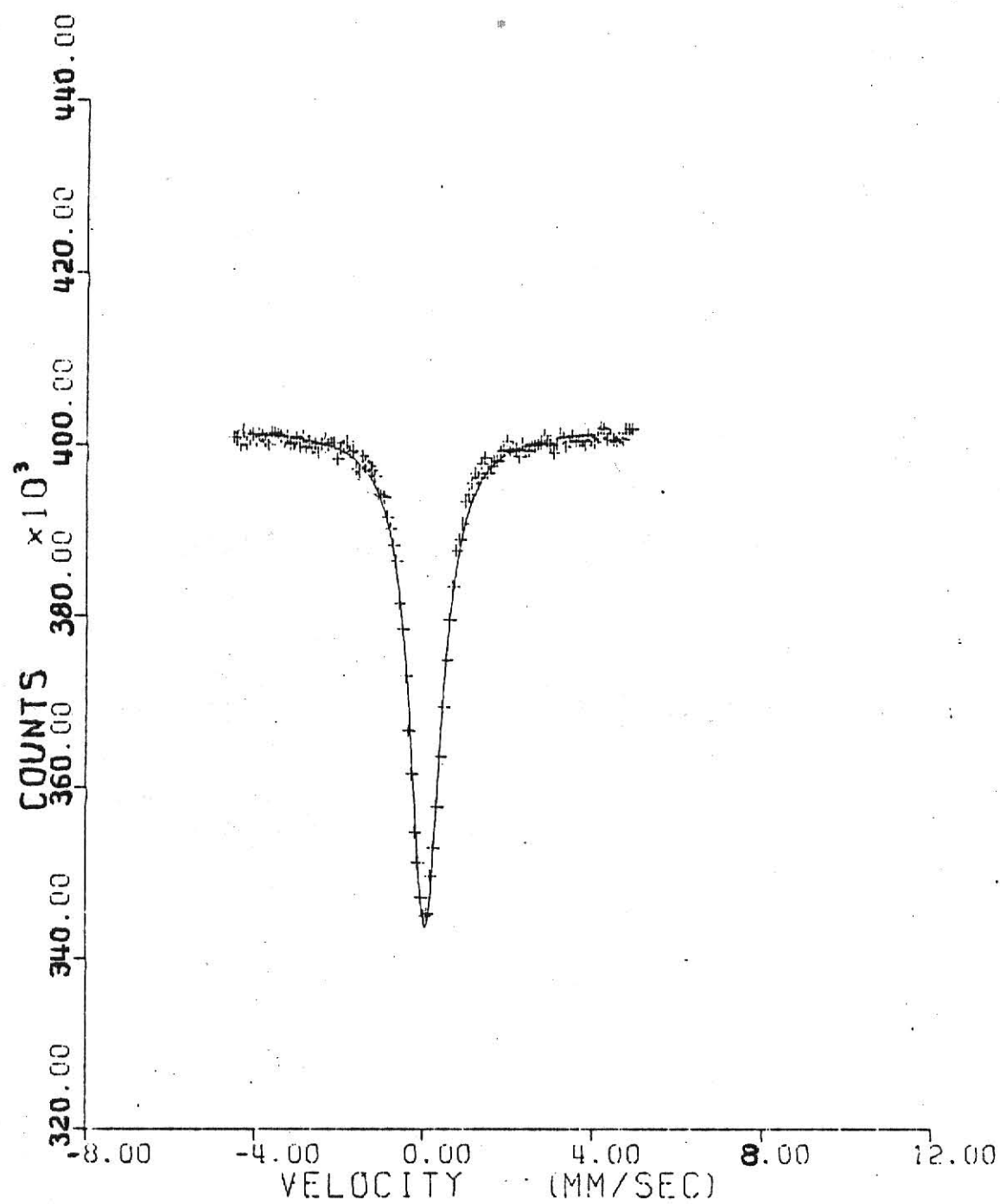


Figure VI. Source - $^{57}\text{Fe}(\text{p,p})^{57}\text{Fe}$; Absorber - ferrocyanide.

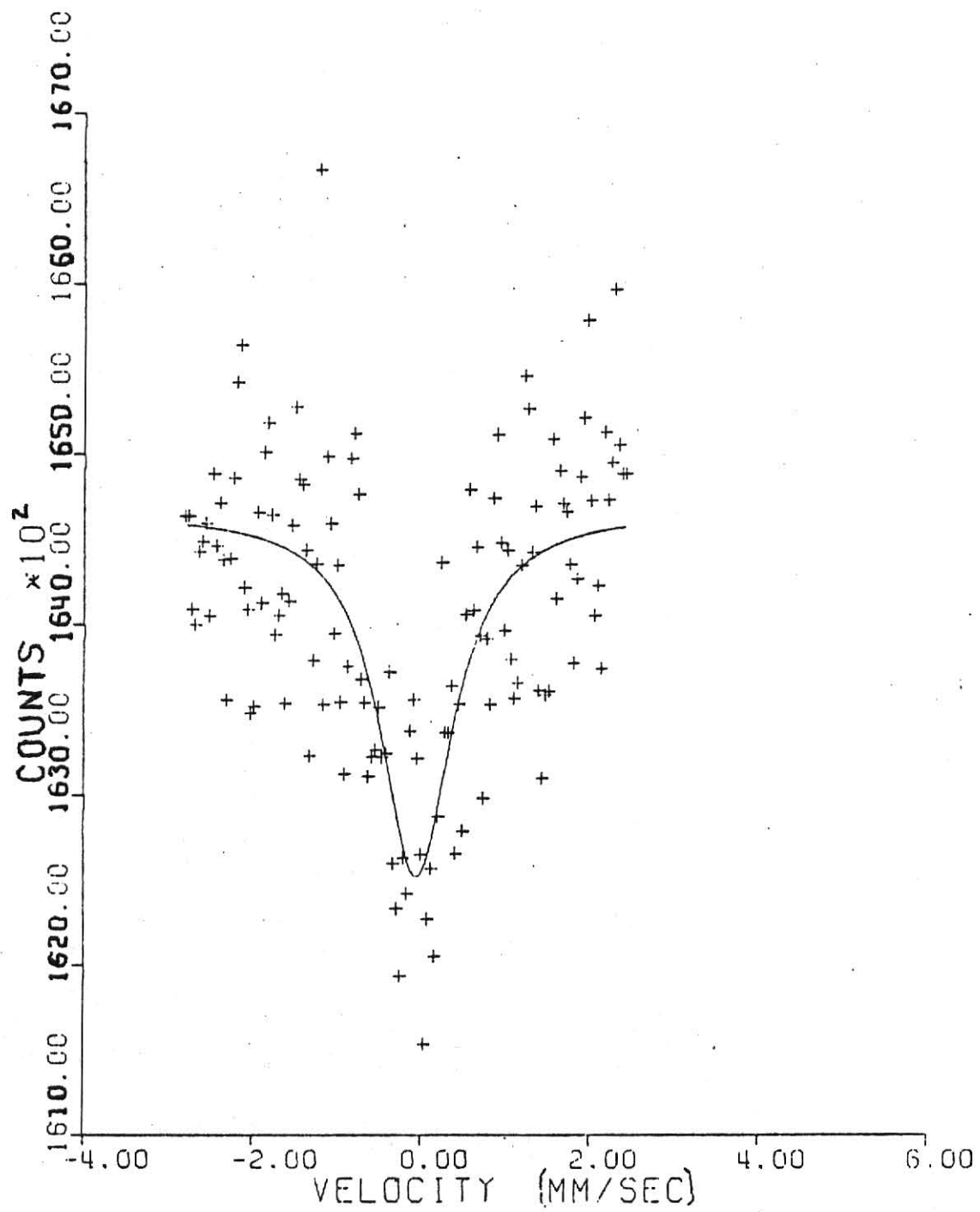


Figure VII. Source - $^{57}\text{Co(Pd)}$; Absorber - irradiated foil.

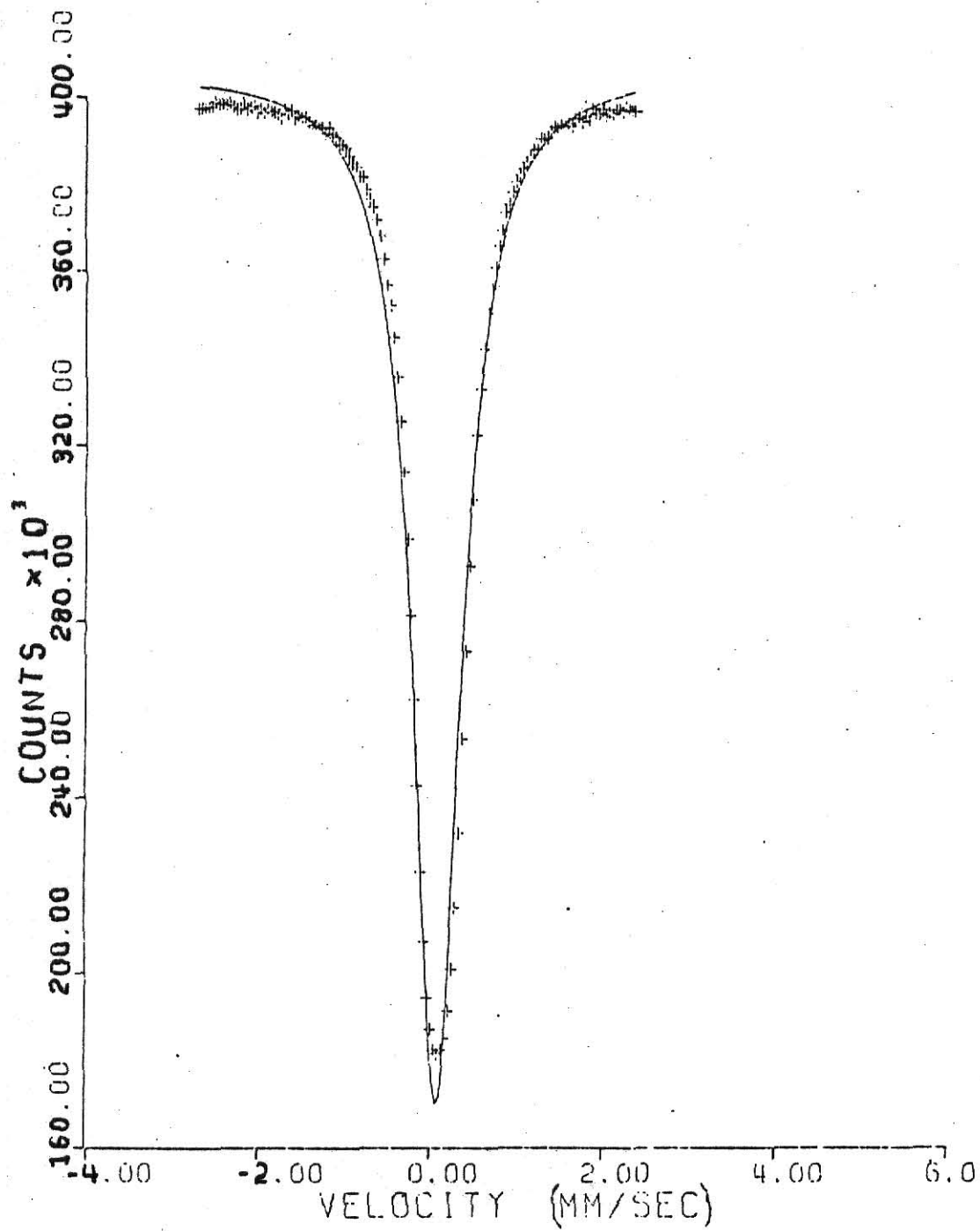


Figure VIII. Source - $^{57}\text{Co(Pd)}$; Absorber - annealed foil.

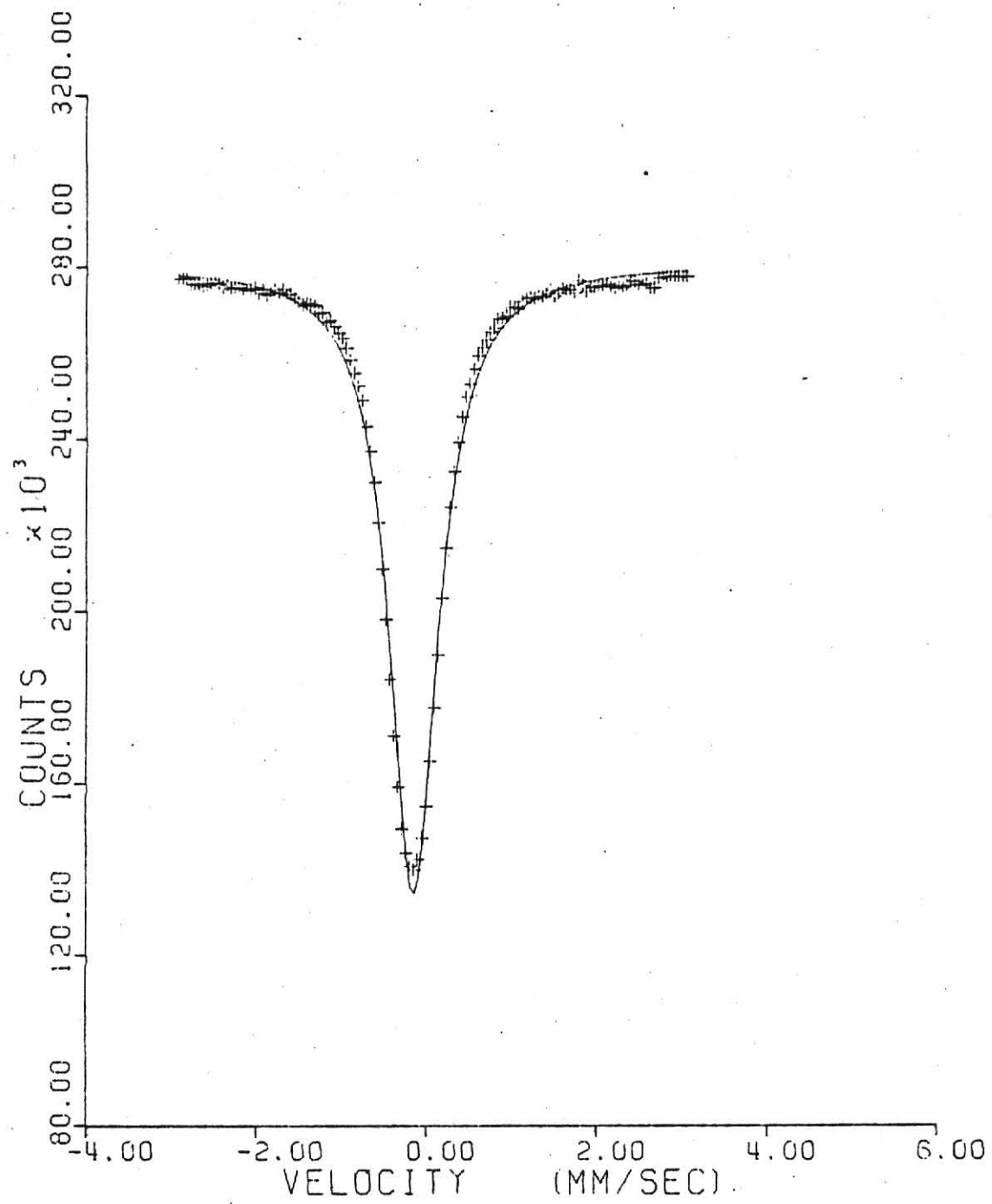


Figure IX. Source - $^{57}\text{Co}(\text{S.S.})$; Absorber - ferrocyanide.

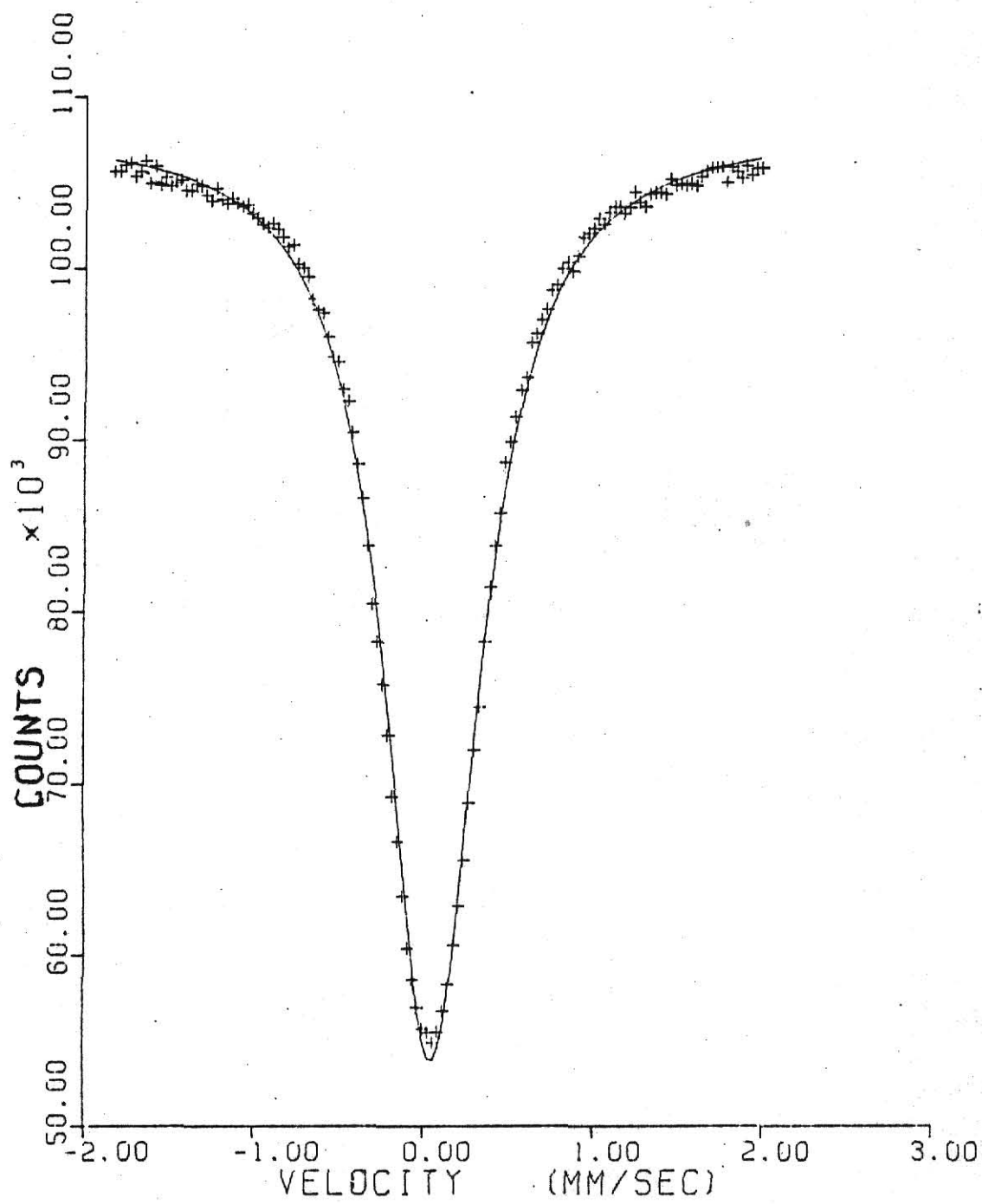
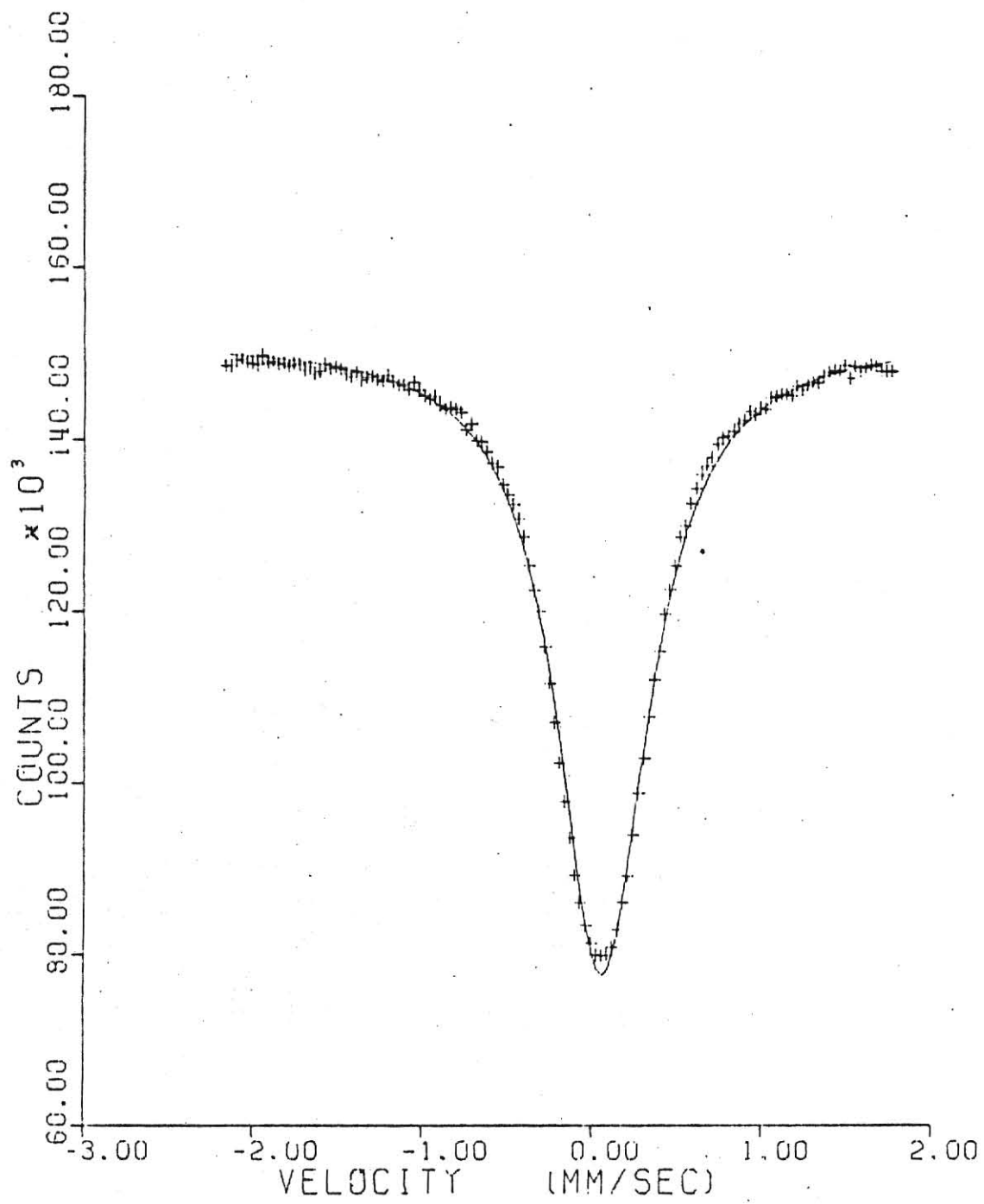


Figure X. Source - $^{57}\text{Co(Pd)}$; Absorber - ferrocyanide.



calibration for the spectrum collected during irradiation was made with a $^{57}\text{Co(Pd)}$ source.

From figures V - X, it is clear that none of the spectra involving the enriched stainless steel foil show any distinguishable magnetic hyperfine splitting, nor any clear electric quadrupole splitting. This indicates that the stainless steel has very little (if any) net internal magnetic field at any time during the proceedings, and that the primary knock-ons very seldom experience any electric field gradient at their final position. The latter point suggests that the primary knock-on comes to rest in a cubic lattice site in almost all cases. As that is one of the findings in the simulations of Vineyard, et al., (Chapter II(a)), their theory is supported to this extent by the experimental results.

It is apparent from the values in Table II(b) that the spectrum taken during irradiation has a far smaller isomer shift than any of the other spectra; its linewidth is greater than that of the other spectra, although not by so great a factor. The large standard deviations of these parameters are due to the scatter of the data points, which is a result of the large number of background counts reaching the analyzer. (By "background" is meant, in this case, counts which are sent through by the SCA but which are not the result of the 14.4 keV gamma ray; "background" normally means the number of counts per channel away from any peaks.) On the other hand, the program is unable to fit closely the minima and shoulders of the peaks in spectra 3 and 4; the widths and positions (hence isomer shifts) are far more reliable than the figures seem to imply.

It may be seen in Table II(b) that the lines which involve stainless steel in either the source or the absorber (or both) are wider than the line which does not use stainless steel in either role (line 6). However, the spectrum taken during irradiation shows a linewidth significantly greater than that of any other spectrum. This broadening could be the result of unresolved quadrupole splitting, or it could be caused by superposition of a range of isomer shifts; as the isomer shift of this spectrum is much different from all the other shifts, and as it seems reasonable that the electron shells would be highly perturbed during irradiation, the broadening of the line in this spectrum is probably due to superposition of different isomer shifts.

The isomer shift is a function of the radii of the ground and excited states of the emitting nucleus, and of the electron density at the nuclei of the emitting and absorbing atoms; specifically, the function is:¹³

$$\begin{aligned} \text{I. S.} &= ((4\pi Ze^2 R_{av}^2/5)(R_{ex} - R_{gd})/(R_{ex} + R_{gd}))(|\psi(0)_A|^2 - |\psi(0)_S|^2) \\ &= \text{constant} \times (|\psi(0)_A|^2 - |\psi(0)_S|^2), \end{aligned} \quad (6)$$

where R_{ex} and R_{gd} are the radii of the emitting nucleus in excited and ground states; R_{av} is the average of these; and $|\psi(0)_A|^2$ and $|\psi(0)_S|^2$ are electron densities at the absorbing and source nuclei, respectively, all of the expression except the electron density terms may be written as a constant because the emitting nucleus is ^{57}Fe for all the spectra involved. Let the constant be identified as C. The $^{57}\text{Co(Pd)}$ source will be called S, while the $^{57}\text{Co(S.S.)}$ source is S'. The absorbers and the foil during irradiation will be identified by abbreviations of their descriptions. For example, the annealed foil is 'annSS'. The isomer shifts from Table II, thus, represent

the following:

TABLE III

$I(1) = C(\psi_{\text{newSS}}^2 - \psi_S^2)$	$I(4) = C(\psi_{\text{annSS}}^2 - \psi_S^2)$
$I(2) = C(\psi_{\text{CN}}^2 - \psi_{\text{bombSS}}^2)$	$I(5) = C(\psi_{\text{CN}}^2 - \psi_S^2)$
$I(3) = C(\psi_{\text{irradSS}}^2 - \psi_S^2)$	$I(6) = C(\psi_{\text{CN}}^2 - \psi_S^2)$

where all ψ^2 above are understood to be abbreviations for $|\psi_N(0)|^2$, where $N = A$ or S . By combining these isomer shifts in appropriate ways, a set of shifts which may be compared directly can be derived. To do this, the following three derived isomer shifts are necessary:

$$I(5') = I(6) - I(5) = C(\psi_S^2 - \psi_S^2),$$

$$I(1') = I(1) + I(5') = C(\psi_{\text{newSS}}^2 - \psi_S^2), \text{ and}$$

$$I(2') = I(6) - I(2) = C(\psi_{\text{bombSS}}^2 - \psi_S^2).$$

Putting in values for the isomer shifts give $I(5') = 0.015$ mm/sec and leads to the following table:

TABLE IV

$I(1') = C(\psi_{\text{newSS}}^2 - \psi_S^2) = 0.109 \pm .007$ mm/sec
$I(2') = C(\psi_{\text{bombSS}}^2 - \psi_S^2) = 0.076 \pm .042$ mm/sec
$I(3) = C(\psi_{\text{irradSS}}^2 - \psi_S^2) = 0.089 \pm .004$ mm/sec
$I(4) = C(\psi_{\text{annSS}}^2 - \psi_S^2) = 0.105 \pm .004$ mm/sec

The preceding table shows that the electron density at the gamma-emitting nuclei appears to be considerably lowered during irradiation; because of the large standard deviation, no clear conclusions may be drawn. If the isomer shift, which can only vary (between the four spectra listed) in the electron density term, has really dropped to 70% of its value for an undamaged foil, then the neighborhood of the emitting nucleus is appreciably changed from its undamaged state. As the disturbances to the inner electronic shells equilibrate in a time less than the half-life of the excited state,³ the decrease of electronic density at the nucleus is probably due to disturbance of the crystal neighborhood (e.g. agitation of neighboring atoms or strains caused by presence of interstitials) or of the conduction electrons. Whatever the ultimate cause, a real change in the isomer shift of this magnitude would indicate a significant change in the lattice during bombardment.

The third isomer shift indicates that the foil has partially self-annealed out whatever internal changes caused the decrease of the isomer shift. The shift has increased to 82% of the value found for the new foil. Therefore, it can be stated that some of the damage anneals out within 18-24 hours at room temperature (about 300°K), but the foil still is clearly in a different condition than it was before irradiation.

After annealing at 394° K for 150 minutes, the foil shows an isomer shift which is essentially the same as that shown by the new foil. This amount of annealing is apparently sufficient to remove all or nearly all effects of the bombardment and to restore the foil to an undamaged (or very slightly damaged) condition.

CONCLUSIONS

This investigation has shown that Coulomb-excited Mössbauer spectroscopy of a stainless steel target under bombardment by energetic protons may be able to yield information on the damage caused to the crystalline structure of the target by the bombardment, even though the target is relatively complex; in this case, the target has a FCC structure with three different kinds of atoms as the major constituents. The data indicate that there are disturbances within the metal during irradiation, but that some of the damage will anneal out spontaneously within a few days at room temperature. This is not true of all the damage, as there was a clear difference between the isomer shifts of the new and irradiated foils; after annealing at a higher temperature, the isomer shifts were approximately the same.

It is also clear that the great majority of primary knock-ons come to rest in cubic lattice sites, even when their initial kinetic energy may be as high as 350 keV. For this point, the simulations of Vineyard, et al., are supported and extended to higher energies.

While Coulomb-excited Mössbauer spectroscopy has been done before, it has always required the use of a gamma-gamma coincidence to bring out the 14.4 keV gamma peak. This necessitated using a second detector and SCA to detect the 122 keV gamma given off when a ^{57}Fe nucleus de-excites from the second excited state to the first. A logic circuit was set such that the MCS could register a count at 14.4 keV only when that count fell within a narrow range of times at the appropriate interval (about 100 nanoseconds) after detection of a 122 keV gamma. This procedure results in a low counting rate.

Energy spectra taken before the irradiation was performed showed that the 14.4 keV peak was clearly observable when a Si(Li) detector was used with an appropriate thickness of aluminum foil shielding between it and the target. It was found that when the special scattering chamber mentioned in Chapter III was used, the Lucite window of the chamber and the supporting plastic in the $\text{NaFe}_2(\text{CN})_6 \cdot 10 \text{H}_2\text{O}$ absorber disc provided the same shielding effect as the optimum thickness of aluminum (about .15 mm). Therefore, no aluminum shielding was used during the irradiation.

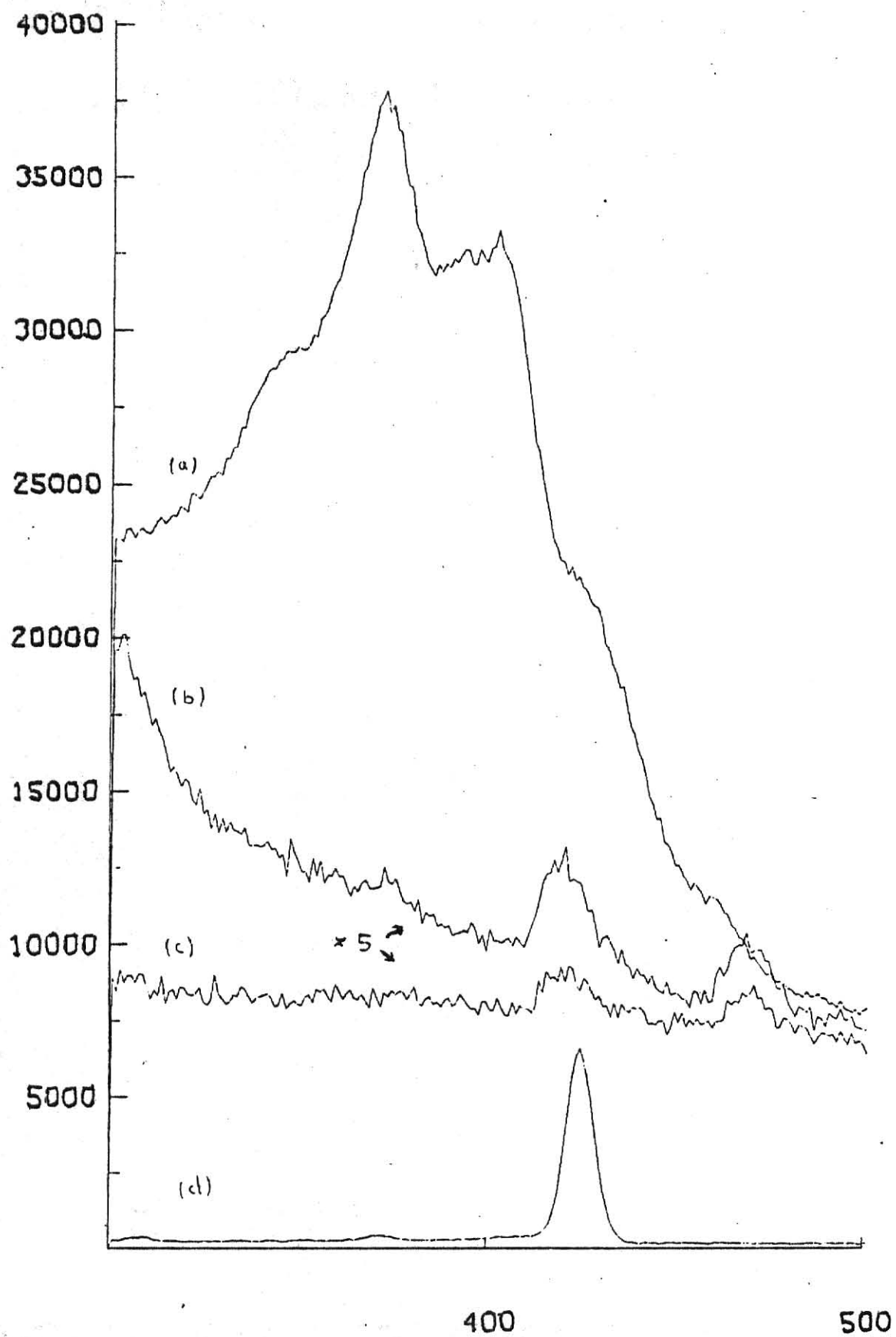
Later calculations and investigations have shown ways in which the spectrum taken during irradiation might be improved. A careful recalculation of the thermal gradient between the beam spot and the edge of the foil has shown that a beam current of 1 microamp should produce a thermal gradient of less than 1°C . Therefore, a beam current 30 times the one actually used should produce no significant heating. A larger beam would produce a higher rate of Coulomb excitations and, hence, a higher count rate.

A series of energy spectra taken with the same stainless steel foil, a proton beam of about 100 nanoamps of 5.0 MeV projectiles, and varying thicknesses of chromium foil between the detector and the target (but without the Mössbauer absorber being in place) shows that a thickness of 0.0127 mm makes the 14.4 keV peak quite prominent relative to its background (see Figure XI). The effect occurs because the major part of the background is due to doubling of Fe K x rays in the detector; the K absorption edge of chromium lies near enough to the energy of the iron K x rays to drastically reduce the count rate, while not seriously

Figure XI. Horizontal axis is channel number (or energy), vertical axis is counts per channel.

- (a) Segment of the spectrum of 5.0 MeV protons on stainless steel; no shielding foil was used. The large peak is the Fe K x-ray doubling peak.
- (b) The same spectrum as (a), except that a .5 mil chromium foil was placed between the target and the detector.
- (c) The same spectrum as (a) and (b), but using a 2.0 mil chromium foil as a shield.
- (d) Segment of the spectrum from a $^{57}\text{Co(Pd)}$ source, showing the location of the 14.4 keV gamma peak.

Spectra (a), (b), and (c) all were made with the same beam current and exposure time.



reducing the count rate of the 14.4 keV gamma rays. As the figure shows, the 2 mil (0.051 mm) foil is thick enough to reduce the 14.4 keV peak appreciably.

The use of higher beam currents and chromium shielding should make it possible to obtain a better spectrum with less scatter in the same running time or less. Further studies of radiation damage to stainless steel by the technique of Coulomb-excited Mössbauer spectroscopy without the need for coincidence circuitry should be feasible; indeed, with appropriate choice of shielding material, it may be possible to extend the technique to any crystalline material containing any element, one of whose isotopes has a low-lying excited state of the nucleus.

APPENDIX: The Program MOSFIT

MOSFIT is a much simplified version of the program M2ASTR; a version of that program was obtained from Johns Hopkins University and modified for use on the IBM 360 by J. S. Eck. The program was then simplified by K. F. Purcell of the Kansas State University, Department of Chemistry.

A precaution must be observed in using this program; the functional subroutines (DATFUN et cetera) call for initial values for certain parameters of each peak, plus background and a solid-angle fitting parameter. For example, DATFUN calls for initial value of background, peak position, peak width, and peak depth (as a fraction of the background), as well as the solid-angle parameter - five variables in all. The number of variables specified must be one less than the number called for, and the solid-angle fitting parameter must not be given. Failure to observe this precaution will result in termination of the computation because of an attempt to divide by 0.

```

C
C      MOSFIT (SIMPLIFIED VERSION OF M2ASTR)
C
C *****
C      INPUT CONSISTS OF:
C      1) (20A4/20A4)  TITLE INFORMATION
C      2) (I4,4A4,F10.0)
C          JX=NC. CHANNELS OF DATA
C          FMT=FCPMAT FOR ENTERING COUNTS
C          ROLL=NC. OF ROLL-OVERS
C      3) (FMT) COUNTS
C      4) (3I10,F10.0)
C          NV=NC. VARIABLES TO BE FIT
C          NL=NO. OF LINES IN SPECTRUM
C          MAXIT=MAX. NO. OF ITERATIONS (DEFAULT=25)
C          ACC='ACCURACY' OF FIT FOR CONVERGENCE TEST
C              (DEFAULT = 0.0001)
C      5) (3L1,8F10.4)
C          LG=LOGICAL VARIABLES TO SELECT DATFUN, DATWUN, OR DATWON
C          V=INITIAL VARIABLES (SEE DATFUN, DATWUN, DATWON)
C      6) (20A4) TITLE FOR PLOT
C      7) (2F10.0)
C          VELMIN=MINIMUM VELOCITY
C          VELCCN=VELOCITY/CHANNEL
C *****
C
COMMON /CMNFIT/  F(512,2),G(32,32),GE(32),MP,MC,MAXIT
COMMON /CMNFUN/  Y(512),W(512),Z(512,2),PI(512),XC(512)
COMMON /CMNVAR/  V(32,2),DV(32),SE(32),NV,VAR,VARI,LOC
COMMON /CMNMAN/  TITLE(40),                LG(3), NL,NF
COMMON /CMNOUT/  POS(25),EPOS(25),WID(25),EWID(25),
1              DEP(25),EDEP(25)
COMMON /CMNINP/  JX,ROLL,ACC

C
C      DIMENSION A(32)
C      LOGICAL LG
C      EXTERNAL DATFUN,DATDIV,DATWUN,DATWIV,DATWON,DATWDV

C      1 CONTINUE

C      *****
C      ZERO VARIABLES
C      *****

DO 20 K=1,512
Y(K)=0
F(K,1)=0
F(K,2)=0
Z(K,1)=0
Z(K,2)=0
20 PI(K)=0
DO 23 K=1,25
PCS(K)=0
EPOS(K)=0
WID(K)=0
EWID(K)=0
DEP(K)=0
EDEP(K)=0
23 CONTINUE

```

```

DO 22 K=1,32
V(K,1)=0
V(K,2)=0
DV(K)=0
SE(K)=0
22 CONTINUE
IT=0

C
C *****
C READ DATA
C *****
C
C CALL INPUT
C
C *****
C SET UP DATA AND WEIGHT MATRICES
C *****
C
ROLL=ROLL*1.E+06
DO 110 I=1,JX
Y(I)=Y(I)+ROLL
W(I)=1/SQRT(Y(I))
110 CONTINUE

C
C *****
C WRITE OUT DATA
C *****
C
115 CONTINUE
WRITE(6,120) (TITLE(I),I=1,20), (TITLE(I),I=21,40)
120 FORMAT(1H1,20A4 /1X,20A4 //)
WRITE(6,125) NF,NV,NL,MAXIT,ACC
125 FORMAT(34H NUMBER OF NON-DROPPED CHANNELS = ,I5/
1 23H NUMBER OF VARIABLES = ,I5/
2 19H NUMBER OF LINES = ,I5/
3 31H MAXIMUM NUMBER OF ITERATIONS = ,I5/
4 11H ACCURACY = ,E9.3//)
132 WRITE(6,135) ROLL,(I,Y(I),I=1,JX)
135 FORMAT(/35X,11H INPUT DATA,
1 31H (INCLUDES ROLLOVER ADDITION CF,F11.0,
2 8H CCUNTS)//(1H.,8(I4,F11.0,1X))

C
C *****
C SET UP VELOCITY ARRAY FOR FIT
C *****
C
DO 49 I=1,NF
XC(I)=FLCAT(I)
49 CONTINUE
50 CONTINUE
IS=1

C
C *****
C WRITE TITLE AND STORE INITIAL V LIST FOR THIS FIT
C *****
C
60 CONTINUE
WRITE(6,120) (TITLE(I),I=1,20), (TITLE(I),I=21,40)
DO 140 I=1,NV
140 A(I) = V(I,1)

```



```

C
C *****
C PLOT DATA AND CALCULATED SPECTRUM
C *****
C
C CALL PLCTIT
C
C *****
C LOOP BACK FOR NEXT DECK
C *****
C
1000 GO TO 1
END
C
C
C SUBROUTINE PLOTIT
C
COMMON /CMNFUN/ Y(512),W(512),Z(512,2),PI(512),XC(512)
COMMON /CMNVAR/ V(32,2),DV(32),SE(32),NV,VAR,VARI,LOC
COMMON/CMNMAN/ TITLE(40),LG(3),NL,NF
COMMON /CMNINP/ JX,RCLL,ACC
DIMENSION XAX(512),IBUF(1000)
C
C TITLE TO APPEAR ON PLOT, LOWEST VELOCITY, AND
C VELOCITY/CHANNEL
C
READ(5,60)(TITLE(I),I=1,20)
60 FORMAT(20A4)
C
READ(5,40) VELMIN,VELCCN
40 FORMAT(2F10.0)
C
XAX(1) = VELMIN
DO 50 I=2,JX
XAX(I) = XAX(I-1) + VELCCN
50 CONTINUE
CALL PLCTS(IBUF,1000)
CALL PLOT(0.0,-11.0,23)
CALL PLOT(2.0,1.5,23)
CALL SCALE(XAX,5.0,JX,1)
CALL SCALE(Y,6.0,JX,1)
IXS = JX + 1
IXE = JX + 2
CALL AXIS(0.0,0.0,16HVELOCITY MM/SEC,-16,5.0,0.0,XAX(IXS),
*XAX(IXE))
*)
CALL AXIS(0.0,0.0,6HCOUNTS,+6,6.0,90.0,Y(IXS),Y(IXE))
CALL LINE(XAX,Y,JX,1,-1,3)
DO 30 I=1,JX
Y(I) = Z(I,LOC)
30 CONTINUE
CALL LINE(XAX,Y,JX,1,0,0)
CALL SYMBOL(0.2,7.0,0.14,TITLE,0.0,30)
CALL PLCT(0.0,0.0,999)
RETURN
END
C
C
C SUBROUTINE INPUT
C

```

```

COMMON /CMNFIT/ F(512,2),G(32,32),GE(32),MP,MC,MAXIT
COMMON /CMNFUN/ Y(512),W(512),Z(512,2),PI(512),XC(512)
COMMON /CMNVAR/ V(32,2),DV(32),SE(32),NV,VAR,VARI,LOC
COMMON /CMNMAN/ TITLE(40), LG(3), NL,NF
COMMON /CMNINP/ JX,RCLL,ACC

C
LOGICAL LG
DIMENSION FMT(4)

C
READ (5,5) TITLE
5 FORMAT(20A4/20A4)

C
READ(5,6) JX,FMT,ROLL
6 FORMAT(I4,4A4,F10.0)
NF=JX

C
READ(5,FMT) (Y(I),I=1,JX)

C
READ(5,7) NV,NL,MAXIT,ACC
7 FORMAT(3I10,F10.0)
IF(ACC.EQ.0) ACC=.0001
IF(MAXIT.EQ.0) MAXIT=25

C
READ(5,9) LG,(V(J,1),J=1,NV)
9 FORMAT(3L1/(8F10.4))

C
*****
C
RESET FIRST AND LAST CHANNEL
C
*****
C

Y(1)=Y(2)
Y(NF)=Y(NF-1)

C
DO 8 I=1,NV
IF(V(I,1).EQ.0.0) V(I,1) = 1.0 E-38
8 CONTINUE
DO 10 I=1,NV
10 DV(I)=ACC*V(I,1)
RETURN
END

C
C
SUBROUTINE FIT (DUMFUN,DUMDIV)

C
COMMON /CMNFIT/ F(512,2),G(32,32),GE(32),MP,MC,MAXIT
COMMON /CMNVAR/ V(32,2),DV(32),SE(32),NV,VAR,VARI,LOC
COMMON /CMNMAN/ TITLE(40), LG(3), NL,NF
DIMENSION DIAG(32),P(32),D(32,2)
DOUBLE PRECISION CHI(2)
LOGICAL LG
LOGICAL JW

C
ITER = -1
JC = 0
JP = 0
MC = 0
LOC = 1
LOC2 = 2
LOC3 = 1
NVL1 = NV-1

```

```

      DEG = NF-NV
      FUDGE = 10.
10  CALL CUMFUN
      CHI(LCC) = 0.
      DO 20 I=1,NF
20  CHI(LCC) = CHI(LCC)+F(I,LCC)**2
      IF (JO.EQ.0) GO TO 46
      IF (CHI(LCC).LT.CHI(LCC2)) GO TO 30
      CHANGE = 0.
      DO 25 I=1,NV
25  CHANGE = AMAX1(ABS(C(I,LCC)/DV(I)/DIAG(I)),CHANGE)
      IF (JP.LE.1.OR.CHANGE.GT..1) GO TO 27
      LCC = LCC2
      FUD = FUDGE
      GO TO 44
27  JP = JP+1
      IF (JP.GT.10.AND.JC.NE.2) GO TO 260
      FUDGE = FUDGE*10.
      LCC3 = LCC2
      LCC2 = LCC
      LCC = LCC3
      IF (JC-1)80,80,40
30  IF (JC.EQ.2.OR.JP.GT.0) GO TO 40
      JO = 2
      IF (FUDGE-2.E-6)40,40,38
38  FUDGE = FUDGE/10.
      LCC = LCC2
      GO TO 80
40  CHANGE = C.
      FUD = FUDGE
      DO 42 I=1,NV
42  CHANGE = AMAX1(ABS(D(I,LCC)/DV(I)/DIAG(I)),CHANGE)
      IF (ITER.LT.MAXIT.AND.CHANGE.GT.1./DG) GO TO 46
44  JO = 3
      FUDGE = 0.
      GO TO 48
46  JO = 1
47  JP = 0
48  ITER = ITER+1
      JW = .FALSE.
      DO 50 I=1,NVL1
      P(I) = 0.
      DIAG(I) = 0.
      DO 50 J=I,NVL1
50  G(J+1,I) = 0.
      P(NV) = 0.
      DIAG(NV) = 0.
      DO 60 I=1,NF
      MP = I
      CALL CUMDIV
56  A = F(I,LCC)*GE(NV)
      P(NV) = P(NV) - A
      DIAG(NV) = DIAG(NV) + GE(NV)**2
      DO 60 J=1,NVL1
      A = F(I,LCC)*GE(J)
      P(J) = P(J) - A
      DIAG(J) = DIAG(J) + GE(J)**2
      DO 60 K=J,NVL1
60  G(K+1,J) = G(K+1,J) + GE(K+1)*GE(J)
      DIAG(1) = SQRT(DIAG(1))

```

```

P(1) = P(1)/DIAG(1)
DO 70 I=2,NV
DIAG(I) = SQRT(DIAG(I))
P(I) = P(I)/DIAG(I)
IL1 = I-1
DO 70 J=1,IL1
70 G(I,J) = G(I,J)/(DIAG(I)*DIAG(J))
80 DG = 1.+FUDGE
DO 85 I=1,NV
DO 85 J=1,I
85 G(J,I) = 0.
G(1,1) = 1./DG
DO 130 L=2,NV
LL1 = L-1
LL2 = LL1-1
IF (LL2.LT.1) GO TO 110
DO 140 I=1,LL2
DO 150 J=I,LL2
G(I,L) = G(I,L)-G(I,J)*G(L,J)
150 G(J+1,L) = G(J+1,L)-G(I,J+1)*G(L,I)
140 G(I,L) = G(I,L)-G(I,LL1)*G(L,LL1)
110 G(LL1,L) = G(LL1,L)-G(LL1,LL1)*G(L,LL1)
B = DG
DO 160 I=1,LL1
160 B = B+G(I,L)*G(L,I)
G(L,L) = 1./B
DO 130 I=1,LL1
BB = G(L,L)*G(I,L)
DO 170 J=I,LL1
170 G(I,J) = G(I,J)+BB*G(J,L)
130 G(I,L) = BB
IF (JW) GO TO 220
VAR = CHI(LOC)/DEG
C
IWRITE=0
C
WRITE (6,200) ITER,MC,VAR,FUD,CHANGE,(V(I,LOC),I=1,NV)
200 FORMAT (//5X,9HITERATION,I4,I9,16H CALLS OF DUMFUN,6X,
2 13H VAR. RATIO =,1PE14.7,6X, 8H FUDGE =,E3.1,6X, 9H CHANGE =,
3 E11.4/4X,11H PARAMETERS /(6E20.7))
210 CONTINUE
IF (JO.EQ.3) GO TO 280
JW = .TRUE.
220 DO 230 I=1,NV
230 D(I,LCC2) = 0.
DO 250 I=1,NVL1
DO 240 J=I,NVL1
D(I,LCC2) = D(I,LCC2) + G(I,J)*P(J)
240 D(J+1,LCC2) = D(J+1,LCC2) + G(I,J+1)*P(I)
D(I,LCC2) = D(I,LCC2) + G(I,NV)*P(NV)
250 V(I,LCC2) = V(I,LCC) + D(I,LCC2) /DIAG(I)
D(NV,LCC2) = D(NV,LCC2) + G(NV,NV)*P(NV)
V(NV,LCC2) = V(NV,LCC) + D(NV,LCC2) /DIAG(NV)
LCC = LCC2
LOC2 = LOC3
LOC3 = LCC
GO TO 10
260 WRITE (6,270)
270 FORMAT (38H THE PROGRAM CANNOT IMPROVE VAR. RATIO)
280 DO 290 I=1,NV

```

```

      DO 290 J=1,I
      G(J,I) = G(J,I)/(DIAG(I)*DIAG(J))
290  G(I,J) = G(J,I)
      CHANGE = 0.
      RETURN
      END

```

SUBROUTINE CATFUN

```

      THIS SUBROUTINE IS REACHED IF LG(1) IS TRUE
      THIS SUBROUTINE FITS TO AN ARBITRARY SUM OF LORENTZIAN
      V(1) = BASELINE
      V(3*J-1) = POSITIONS, V(3*J) = WIDTHS, V(3*J+1) = DEPTHS
      V(3*NL+2) = SOLID ANGLE CORRECTION PARAMETER

```

```

      COMMON /CMNFIT/ F(512,2),G(32,32),GE(32),MP,MC,MAXIT
      COMMON /CMNFUN/ Y(512),W(512),Z(512,2),PI(512),XC(512)
      COMMON /CMNVAR/ V(32,2),DV(32),SE(32),NV,VAR,VARI,LCC
      COMMON /CMNMAN/ TITLE(40), LG(3), NL,NF
      LOGICAL LG

```

```

      MC = MC+1
      DO 5 I=1,NF
      S = 0.
      DO 10 J=1,NL
10  S = S + V(3*J+1,LCC)/(((XC(I) - V(3*J-1,LCC))/V(3*J,
      LLOC))**2+1.)
      Z(I,LCC) = V(1,LCC)*(1.-S) + V(3*NL+2,LCC) * PI(I)
      5  F(I,LCC) = W(I)*(Z(I,LCC)-Y(I))
      RETURN
      ENTRY DATCIV
      DF = 0.
      DO 20 I=1,NL
      E = (V(3*I-1,LCC)-XC(MP))/V(3*I,LCC)
      FE = 1./(1.+E*E)
      FW = FE*W(MP)
      GE(3*I+1) = -V(1,LCC)*FW
      GE(3*I-1) = -2.*GE(3*I+1)* V(3*I+1,LCC) *FE*E/V(3*I,LCC)
      GE(3*I) = -GE(3*I-1)*E
20  DF = DF + V(3*I+1,LCC)*FW
      GE(3*NL+2) = W(MP)*PI(MP)
      GE(1) = W(MP) -DF
      RETURN
      END

```

SUBROUTINE DATWUN

```

      THIS SUBROUTINE IS REACHED IF LG(2) IS TRUE
      V(1)=BASELINE,V(2)=WIDTH,V(2*J+1)=POSITION,V(2*J+2)=DEPTH
      V(2*NL+3)=SOLID ANGLE CORRECTION PARAMETER

```

```

      COMMON /CMNFIT/ F(512,2),G(32,32),GE(32),MP,MC,MAXIT
      COMMON /CMNFUN/ Y(512),W(512),Z(512,2),PI(512),XC(512)
      COMMON /CMNVAR/ V(32,2),DV(32),SE(32),NV,VAR,VARI,LCC
      COMMON /CMNMAN/ TITLE(40), LG(3), NL,NF
      LOGICAL LG

```

```

      MC = MC+1

```

```

DO 5 I=1,NF
S = 0.
DO 10 J=1,NL
10 S = S + V(2*J+2,LCC)/(((XC(I) - V(2*J+1,LCC))/V(2 ,
1LCC))**2 + 1.)
Z(I,LCC) = V(1,LCC)*(1.-S) + V(2*NL+3,LCC) * PI(I)
5 F(I,LCC)= W(I)*(Z(I,LCC)-Y(I))
RETURN
ENTRY CATWIV
DF = 0.
GE(2) = 0.
DO 20 I=1,NL
E = (V(2*I+1,LCC)-XC(MP))/V(2 ,LCC)
FE = 1./(1.+E*E)
FW = FE*w(MP)
GE(2*I+2) = -V(1,LCC)*FW
GE(2*I+1) = -2.*GE(2*I+2)* V(2*I+2,LCC) *FE*E/V(2 ,LCC)
GE(2) = GE(2) - GE(2*I+1)*E
20 DF = DF + V(2*I+2,LCC)*FW
GE(2*NL+3) =W(MP)*PI(MP)
GE(1) = W(MP) -DF
RETURN
END

```

C
C

SUBROUTINE CATWDN

C
C
C
C
C
C
C
C
C

THIS SUBROUTINE IS REACHED IF LG(3) IS TRUE
THIS SUBROUTINE FITS TO A SUM OF LORENTZIAN WITH EQUAL
WIDTHS AND DEPTHS.
V(1) = BASELINE, V(2) = WIDTH, V(3) = DEPTH,
V(J+3) = POSITION,
V(NL+4) = SOLID ANGLE CORRECTION PARAMETER

```

COMMON /CMNFIT/ F(512,2),G(32,32),GE(32),MP,MC,MAXIT
COMMON /CMNFUN/ Y(512),W(512),Z(512,2),PI(512),XC(512)
COMMON /CMNVAR/ V(32,2),DV(32),SE(32),NV,VAR,VARI,LOC
COMMON /CMNMAN/ TITLE(40), LG(3), NL,NF
LOGICAL LG

```

C

```

MC = MC+1
DO 5 I=1,NF
S = 0.
DO 10 J=1,NL
10 S = S + V(3,LCC)/(((XC(I) - V(J+3,LCC))/V(2,LCC))**2 + 1.)
Z(I,LCC) = V(1,LCC)*(1.-S) + V(NL+4 ,LCC) * PI(I)
5 F(I,LCC) = W(I)*(Z(I,LCC)-Y(I))
RETURN
ENTRY DATWDV
DF = 0.
GE(2) = 0.
GE(3) = 0.0
DO 20 I=1,NL
E = (V(I+3 ,LCC)-XC(MP))/V(2 ,LCC)
FE = 1./(1.+E*E)
FW = FE*w(MP)
GED = -V(1,LCC)*FW
GE(3) = GE(3) + GED
GE(I+3) = -2.*GED*V(3,LCC)*FE*E/V(2,LCC)
GE(2) = GE(2) - GE(I+3) *E

```

```

20 DF = DF + V(3,LCC)*FW
   GE(NL+4) = W(MP)*PI(MP)
   GE(1) = W(MP) -DF
   RETURN
   END

```

C
C

SUBROUTINE DATOUT

C

```

COMMON /CMNFIT/ F(512,2),G(32,32),GE(32),MP,MC,MAXIT
COMMON /CMNFUN/ Y(512),W(512),Z(512,2),PI(512),XC(512)
COMMON /CMNVAR/ V(32,2),DV(32),SE(32),NV,VAR,VARI,LOC
COMMON /CMNMAN/ TITLE(40), LG(3), NL,NF
COMMON /CMNOUT/ POS(25),EPOS(25),WID(25),EWID(25),
* DEP(25),EDEP(25)
COMMON /CMNINT/ INT(25),EINT(25)
REAL INT
LOGICAL LG

```

C
C
C

SET UP POSITION, WIDTH, AND DEPTH MATRICES

```

100 DO 1070 J=1,NL
    IF(LG(1 )) GO TO 200
    IF(LG(2 )) GO TO 300
    IF(LG(3 )) GO TO 400
200 IP = 3*J-1
210 IW = 3*J
220 ID = 3*J+1
230 IPA = 3*NL+2
240 GO TO 1000
300 IP = 2*J+1
310 IW = 2
320 ID = 2*J+2
330 IPA = 2*NL+3
340 GO TO 1000
400 IP = J+3
410 IW = 2
420 ID = 3
430 IPA = NL + 4
440 GO TO 1000
1000 POS(J) = V(IP,LCC)
1010 EPOS(J) = SE(IP)
1020 WID(J) = V(IW,LCC)
1030 EWID(J) = SE(IW)
1050 DEP(J) = V(ID,LOC)
1060 EDEP(J) = SE(ID)
1070 CONTINUE

```

C
C
C

COMPUTE INTENSITIES

2000 CALL INTENS

C
C
C

WRITE PARAMETERS

```

WRITE(6,120) (TITLE(I),I=1,20), (TITLE(I),I=21,40)
120 FORMAT(1H1,20A4 /1X,20A4 ///)
2120 IF(LG(1 )) WRITE(6,2130)
2130 FORMAT(60H FIT ASSUMES LINES HAVE ARBITRARY POSITION,
1 WIDTH, AND DEPTH//)
2140 IF(LG(2 )) WRITE(6,2150)

```

```

2150 FORMAT(70H FIT ASSUMES ALL WIDTHS ARE EQUAL. POSITIONS
      1 AND DEPTHS ARE ARBITRARY.//)
2160 IF(LG(3)) WRITE(6,2170)
2170 FORMAT(70H FIT ASSUMES ALL WIDTHS AND DEPTHS ARE EQUAL.
      1 POSITIONS ARE ARBITRARY.//)
2300 WRITE(6,2310) VAR,V(1,LCC),SE(1)
2310 FORMAT(17H VARIANCE RATIO =,F10.5//
      1 11H BASELINE =,F11.0,5X,1H(,F8.0,1H)//)
2320 WRITE(6,2330)
2330 FORMAT(5H LINE,7X,8HVELOCITY,17X,5HWIDTH,18X,5HDEPTH,16X,
      1 9HINTENSITY//)
2340 WRITE(6,2350) (I,POS(I),EPOS(I),WID(I),EWID(I),DEP(I),EDEP(I),
      1 INT(I),EINT(I),I=1,NL)
2350 FORMAT((I5,4(F10.4,2F(,E7.1,4H) )))
2360 CONTINUE
2500 WRITE(6,2510)
2510 FORMAT(1H1)
      RETURN
      END

```

C
C

SUBROUTINE INTENS

C

```

COMMON /CMNFIT/ F(512,2),G(32,32),GE(32),MP,MC,MAXIT
COMMON /CMNFUN/ Y(512),W(512),Z(512,2),PI(512),XC(512)
COMMON /CMNVAR/ V(32,2),DV(32),SE(32),NV,VAR,VARI,LOC
COMMON /CMNMAN/ TITLE(40), LG(3), NL,NF
COMMON /CMNCUT/ PCS(25),EPOS(25),WID(25),EWID(25),
* DEP(25),EDEP(25)
COMMON /CMNINT/ INT(25),EINT(25)
REAL INT
LOGICAL LG

```

C

C

C

C

C

C

C

C

C

C

C

C

C

C

C

C

C

C

C

C

C

C

C

C

C

C

C

C

C

C

C

C

C

C

```

100 TINT = 0.0
110 ETINT = 0.0

```

SUM OVER LINES

```

200 DO 260 J=1,NL
      INT(J)=ABS(DEP(J)*WID(J))
240 TINT = TINT + INT(J)
      EINT(J)=INT(J)*SQRT((EDEP(J)/DEP(J))**2+(EWID(J)/WID(J))**2)
      ETINT=ETINT+EINT(J)*EINT(J)
260 CONTINUE

```

ETINT=SQRT(ETINT)

MAKE INTO FRACTIONS

```

300 DO 320 J=1,NL
      A=EINT(J)/INT(J)
      B=ETINT/TINT
310 INT(J) = INT(J)/TINT

```

```
EINT(J)=INT(J)*SQRT(A*A+B*B)  
320 CONTINUE  
RETURN  
END
```

NOTES

1. F. L. Book, "Effects of Radiation on Materials", Phys. Today 28, No. 9, p. 34.
2. G. K. Wertheim, Mössbauer Effect, p. 13.
3. Conversation with B. Curnutte.
4. Y. K. Lee, et al., Phys. Rev. Lett. 14:957; later papers on this experiment are D. A. Goldberg, et al., Phys. Lett. 20:571 and E. T. Ritter, et al., Phys. Rev. 154:287.
5. J. B. Gibson, et al., Phys. Rev. 120:1229.
6. C. Erginsoy, et al., Phys Rev. 133:A595.
7. C. Erginsoy, et al., Phys. Rev. 139:A118.
8. Conversation with R. D. Dragsdorf; also "Austenite: A face-centered cubic, iron-rich solid solution containing carbon (and possibly other elements)", from Moffatt, Pearsall, and Wulff, p.197".
9. Handbook of Chemistry and Physics, 53 Edition, p. F-131.
10. I. B. Gibson, et al., Phys. Rev. 120, 1233f.
11. Wertheim, Mössbauer Effect, p. 60.
12. K. Alder, et al., Rev. Mod. Phys. 28:432.
13. For example, Williamson, Boujot, and Picard or Northcliffe and Schilling.
14. P. G. Debrunner and H. Frauenfelder, in L. May (ed.), An Introduction to the Mossbauer Effect, p. 21.
15. Wertheim, Mössbauer Effect, p. 52.

BIBLIOGRAPHY

- K. Alder, A. Bohr, T. Huus, B. Mottelson, and A. Winther; "Study of Nuclear Structure by Electromagnetic Excitation with Accelerated Ions", Rev. Mod. Phys. 28,432 (1956).
- C. Erginsoy, G. H. Vineyard, and A. Englert, "Dynamics of Radiation Damage in a Body-centered Cubic Lattice", Phys. Rev. 133, A595 (1964).
- C. Erginsoy, G. H. Vineyard, and A. Shimizu, "Dynamics of Radiation Damage in a Body - Centered Cubic Lattice. II. Higher Energies", Phys. Rev. 139,A118 (1965).
- H. Frauenfelder, The Mössbauer Effect, New York: W. A. Benjamin, Inc. (1963).
- J. B. Gibson, A. N. Goland, M. Milgram, and G. H. Vineyard, "Dynamics of Radiation Damage", Phys. Rev. 120, 1229 (1960).
- D. A. Goldberg, Y. K. Lee, E. T. Ritter, R. R. Stevens, Jr., and J. C. Walker, "Relevance of Bombardment-Induced Mössbauer Effects in Iron to Radiation Damage Theories", Phys. Lett. 20, 571 (1966).
- R. S. Hardwell, "Radiation Damage in Metals and Semiconductors" in (H. S. Dupuy Let) Radiation Damage Processes in Materials, Leyden: Nordhoff International Publishing (1975).
- G. Lang, "Interpretation of Experimental Mössbauer Spectrum Areas", Nuc. Inst. and Meth. 24, 425 (1963).

C. M. Lederer, J. M. Hollander, and I. Perlman, Table of Isotopes, Sixth Edition, New York:Wiley and Sons (1968).

Y. K. Lee, P. W. Keaton, Jr., E. T. Ritter, and J. C. Walker, "Mössbauer Effect from Coulomb-Excited Levels in Fe^{57} ", Phys. Rev. Lett. 14, 957 (1965).

L. May (Ed.), An Introduction to Mössbauer Spectroscopy, New York: Plenum Press (1971).

W. G. Moffatt, G. W. Pearsall, and J. Wulft, Structure (Vol. I of Structure and Properties of Materials), New York:Wiley and Sons (1964).

L. C. Northcliffe and R. F. Schilling, "Range and Stopping-Power Tables for Heavy Ions", Nuclear Data Tables, A7, 233 (1970).

E. T. Ritter, P. W. Keaton, Jr., Y. K. Lee, R. R. Stevens, Jr., and J. C. Walker, "Mössbauer Effect Following Coulomb Excitation of Fe^{57} ", Phys. Rev. 154, 287 (1967).

D. A. Shirley, M. Kaplan, and P. Axel, "Recoil-free Resonant Absorption in Au^{197} ", Phys. Rev. 123, 816 (1961).

D. Seyboth, F. E. Obenshain, and G. Czjzek, "Observation of Recoilless Emission of ^{61}Ni Gamma Rays Following Coulomb Excitation", Phys. Rev. Lett. 11, 954 (1965).

M. F. Thomas and M. A. Grace, "Coulomb Excitation of the 14.4 keV State in Fe^{57} ", Phys. Lett. 10, 306 (1964).

G. Vogl, A. Schaefer, W. Mansel, J. Prechtel, and W. Vogl, "Mössbauer Studies of Low-temperature Radiation Damage in α -Iron", Phys. Stat. Sol. (b) 59, 107 (1973).

F. L. Vook, "Effects of Radiation on Materials", Phys. Today, 28, No. 9 p. 34 (1975).

L. R. Walker, G. K. Wertheim, and V. Jaccarino, "Interpretation of the Fe^{57} Isomer Shift", Phys. Rev. Lett. 6, 98 (1961).

G. K. Wertheim, Mössbauer Effect: Principles and Applications, New York: Academic Press (1964).

G. K. Wertheim, "Measurement of Local Fields at Impurity Fe^{57} Atoms Using the Mössbauer Effect", Phys. Rev. Lett. 4, 403 (1960).

G. K. Wertheim, "Mössbauer Effect: Applications to Magnetism", J. Appl. Phys. 32, 110S (1961).

C. F. Williamson, J. P. Boujot, and J. Picard, Tables of Range and Stopping Power of Chemical Elements for Charged Particles of Energy U. S. to 500 MeV, Rapport CEA-R-3042, Sanclay: Centre d'Etudes Nucleaire (1966).

STUDY OF RADIATION DAMAGE IN STAINLESS STEEL
BY COULOMB-EXCITED MOSSBAUER SPECTROSCOPY

by

JAMES NILS WICKBERG

B. S. in Physics, Oklahoma University, 1974

AN ABSTRACT OF A MASTER'S THESIS

submitted in partial fulfillment of the
requirements for the degree

MASTER OF SCIENCE

Department of Physics

KANSAS STATE UNIVERSITY
Manhattan, Kansas

1977

The damage to stainless steel caused by energetic particles, which is a matter of importance to the design of fission and fusion reactors, was studied in this investigation. A stainless steel foil (type 310, 91% enriched with ^{57}Fe) was irradiated with a beam of 5.0 MeV protons, causing radiation damage to the foil and also Coulomb-exciting the ^{57}Fe nuclei. The de-excitation of these nuclei involves emission of a 14.4 keV gamma ray in some cases; during the irradiation, this peak was observed with a Si(Li) detector and a Mössbauer spectrum was collected from the direct spectrum, using a loudspeaker drive and a $\text{NaFe}_2(\text{CN})_6$ absorber. This spectrum was compared with spectra of the same foil taken before and after irradiation, and after annealing. It was found that there is a significant change in the Mössbauer spectrum during irradiation and that part of this change vanished spontaneously within one day after irradiation when the foil is kept at room temperature; annealing at 395°K for 150 minutes restored the spectrum to its initial form. The spectrum taken during irradiation indicated by its lack of separable electric quadrupole splitting that the excited atoms - the "primary knock-ons" - are in nearly cubic lattice sites at de-excitation. This supports the computer simulations of Vineyard, et al. Methods by which the present technique could be improved are suggested.